

# Electrodermal activity as a proxy for sweat rate monitoring during physical and mental activities

Received: 6 May 2024

Accepted: 26 February 2025

Published online: 1 April 2025

 Check for updates

Seung-Rok Kim  <sup>1,2,3,6</sup>, Yifei Zhan  <sup>1,6</sup>, Noelle Davis <sup>1,2,3,6</sup>, Suhirth Bellamkonda <sup>1</sup>, Liam Gillan  <sup>4</sup>, Elina Hakola <sup>5</sup>, Jussi Hiltunen  <sup>5</sup> & Ali Javey  <sup>1,2,3</sup>✉

Electrodermal activity has long been used for mental activity monitoring by measuring skin conductance at specific locations, such as fingertips, with high sweat gland density. However, electrodermal activity has not been considered useful for physical activity monitoring, where large sweat volumes are generated, resulting in the accumulation of sweat at the skin–electrode interface and, thus, preventing further dynamic response to sweating events. Here we show that electrodermal activity can be used as a proxy for sweat loss measurement under both low and high physical activity levels. We use wearable sweat sensors that consist of water-permeable electrodes and microfluidic-based sweat analysers, and show that skin conductance is proportional to the instantaneous sweat loss. We demonstrate that sweat loss during exercise can be estimated by integrating skin conductance over time, which can be applied to assess the body hydration status of exercisers. From multisite measurements of skin conductance, we show that the wrist, forearm and upper arm are reflective of physical activity levels, whereas the finger is indicative of mental activity. Simultaneous measurement of two different sites selectively decouples mental and physical activities.

The autonomic nervous system regulates involuntary physiological processes for homeostasis in response to physical and mental activities<sup>1,2</sup>. Wearable biosensors for physiological signals such as heart rate, blood pressure, body temperature and sweat secretion rate can, thus, be used to monitor a person's physical or mental state<sup>3–6</sup>. However, psychological activities induce relatively small physiological changes and are difficult to detect compared with physical activities<sup>7</sup>. Nevertheless, electrodermal activity (EDA) has long been used for psychological stress or excitement by measuring skin conductance (SkinG) at specific locations with high sweat gland density, such as the fingers, soles of the feet and forehead<sup>8–10</sup>. During mental activities, SkinG consists of a long-lasting, slowly drifting baseline (tonic, SkinG level) overlaid

by short-term, subtle pulses (phasic, SkinG response)<sup>8,11</sup>. Because the phasic component represents signalling by the sympathetic nerve system—leading to the filling and release of the sweat gland—clinicians have used it to analyse mental activity<sup>8</sup>.

Given its simple and robust sensing mechanism, EDA has proven to be of value in various medical and consumer electronic products<sup>12</sup>. In theory, EDA could also be used for measuring sweat rates at rest as well as during physical activity, as SkinG is a measure of skin hydration, which, in turn, is related to the sweat rate<sup>13,14</sup>. However, various studies have shown the limitations of EDA for tracking physical activity<sup>15–19</sup> (Supplementary Note 1). Specifically, during physical activities and/or extended usage, large sweat volumes are generated and trapped at

<sup>1</sup>Department of Electrical Engineering and Computer Sciences, University of California, Berkeley, CA, USA. <sup>2</sup>Materials Sciences Division, Lawrence Berkeley National Laboratory, Berkeley, CA, USA. <sup>3</sup>Berkeley Sensor and Actuator Center, University of California, Berkeley, CA, USA. <sup>4</sup>VTT Technical Research Centre of Finland Ltd, Espoo, Finland. <sup>5</sup>VTT Technical Research Centre of Finland Ltd, Oulu, Finland. <sup>6</sup>These authors contributed equally: Seung-Rok Kim, Yifei Zhan, Noelle Davis. ✉e-mail: [ajavey@berkeley.edu](mailto:ajavey@berkeley.edu)

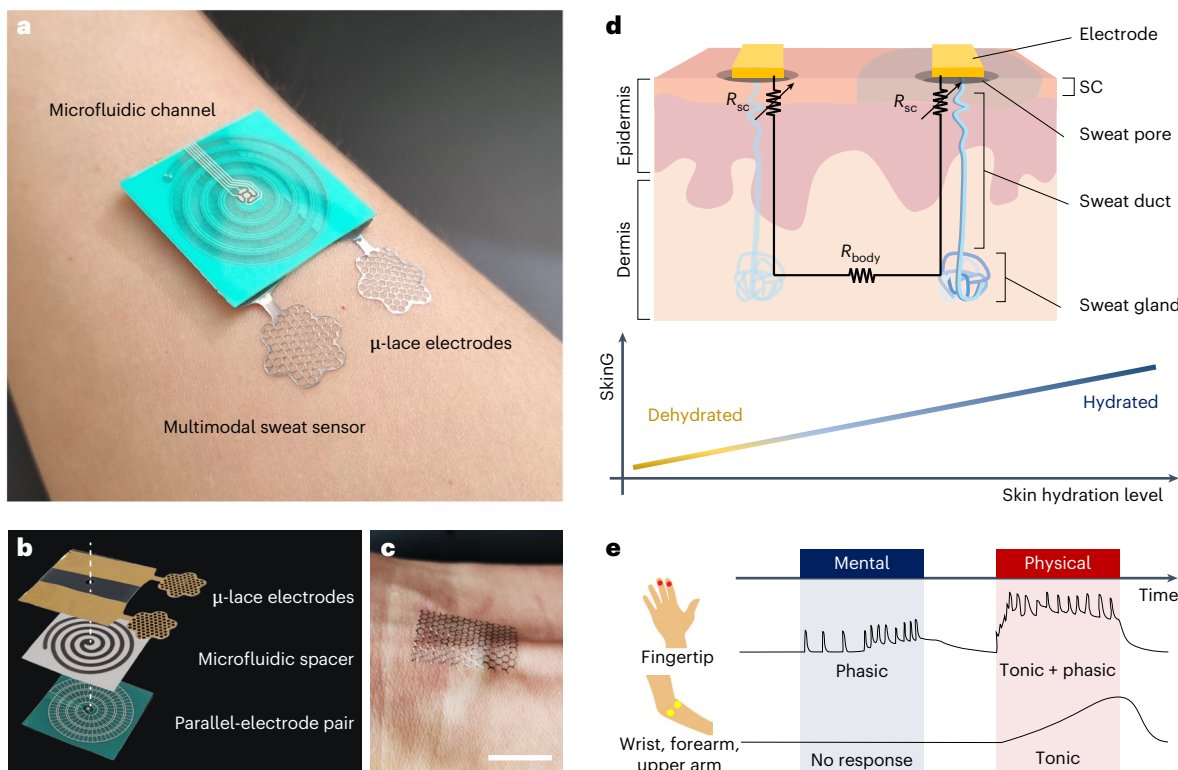


**Fig. 1 | Images and schematic of the multimodal sweat sensor for monitoring mental and physical activities.** **a**, Photograph showing the SkinG sensor with  $\mu$ -lace electrodes integrated with the microfluidic channel for multimodal sweat sensing on the participant's forearm. **b**, Laminated components of the integrated

device. **c**, Photograph of the conformal  $\mu$ -lace electrode on the tendons of the wrist. Scale bar, 1 cm. **d**, Schematic of the skin hydration model for SkinG. **e**, Different SkinG responses from the body sites with different amounts of sweat gland densities for deconvolution of mental and physical activities.

the skin-electrode interface<sup>20,21</sup>. This results in maximum hydration of the skin under the electrode, and thus high SkinG, without further sensitivity to the instantaneous changes in sweat rate. Furthermore, the skin under the electrode can physically deform on extended wear of the electrodes due to the sweat trapped at the interface, which can, in turn, affect the function of the local sweat glands<sup>22</sup>.

In this Article, we show that EDA can be used as a proxy for local sweat secretion rate with the help of water-permeable electrodes with different structures and form factors. In one system, dry electrodes fabricated on thin plastic substrates are laser cut into a lace-like structure with sub-50- $\mu$ m linewidths, smaller than the average size of sweat pores<sup>23</sup>. This design allows sweat to be readily removed from the skin interface, without accumulation at the interface. We use this approach to fabricate multimodal sensing patches, consisting of a microfluidic-based sweat rate sensor with microlace ( $\mu$ -lace) electrodes. We perform detailed participant studies, demonstrating a strong correlation between SkinG and sweat rate on the forearm. We also provide a promising method for monitoring hydration status during high-intensity exercise based on the positive correlation between the integral of relative SkinG change and total sweat loss under high physical activity levels. Furthermore, we perform multi-site measurements to map the variation in SkinG response with the body site. Although fingertips respond to both physical and mental activities, wrists, forearms and upper arms are shown to exhibit a response strongly dominated by physical activity. Thus, both mental and physical activities can be independently monitored using multisite measurements.

## Structural design and modelling of multimodal sweat sensor

Our multimodal sweat sensor consists of  $\mu$ -lace electrodes and a microfluidic channel, and allows the continuous and simultaneous

measurement of SkinG and sweat rate (Fig. 1a). Although the microfluidic sweat sensor measures the progressing volume of locally secreted sweat, the SkinG system continuously measures the local hydration state of the skin with two paired electrodes on the skin. The  $\mu$ -lace electrodes consist of titanium (50 nm thickness) and gold (100 nm thickness) deposited sequentially on top of 10- $\mu$ m polyethylene terephthalate. The skin-contacting areas of the electrodes were laser patterned for water permeability. We anchored  $\mu$ -lace electrodes on the skin with permeable self-adhesive bandage (Supplementary Fig. 1). As shown in Fig. 1b, the SkinG sensing  $\mu$ -lace electrodes can be easily combined with a microfluidic sweat rate sensor by laminating the electrodes onto the microfluidic channel. Thin and flexible  $\mu$ -lace electrodes showed conformal contact with the bumpy tendons of the wrist (Fig. 1c).

To relate SkinG to the skin hydration level, we assumed the electrical model of the skin (Fig. 1d and Supplementary Note 2). By applying a direct-current voltage across two electrodes directly connected to the skin, we can measure the total electrical resistance (1/conductance;  $R$ ) across the regions of electrode contacts, stratum corneum (SC), epidermis and dermis, involving sweat glands, interstitial fluid and vascularization. The internal body resistance  $R_{body}$  is only a few hundreds of ohms, which is a few orders of magnitude smaller than  $R_{sc}$ . Thus, the total measured resistance is given by that of SC with  $\text{SkinG} = 1/(2R_{sc})$ . Because SkinG increases from the dehydrated state to the hydrated state of the SC<sup>13</sup>, we can correlate the total amount of locally secreted sweat to the amount of sweat absorbed in the SC during hydration. Using this modelling involving skin hydration level, we can use tonic SkinG as a proxy for local sweat rate monitoring.

Our SkinG sensor can selectively monitor mental and physical activities because different skin sites show different SkinG responses (Fig. 1e)<sup>10</sup>. As in typical EDA analysis, we can obtain phasic responses of SkinG from mental stimulus on skin sites with high sweat gland density, such as the distal fingertip phalanges, palms, soles of the feet and

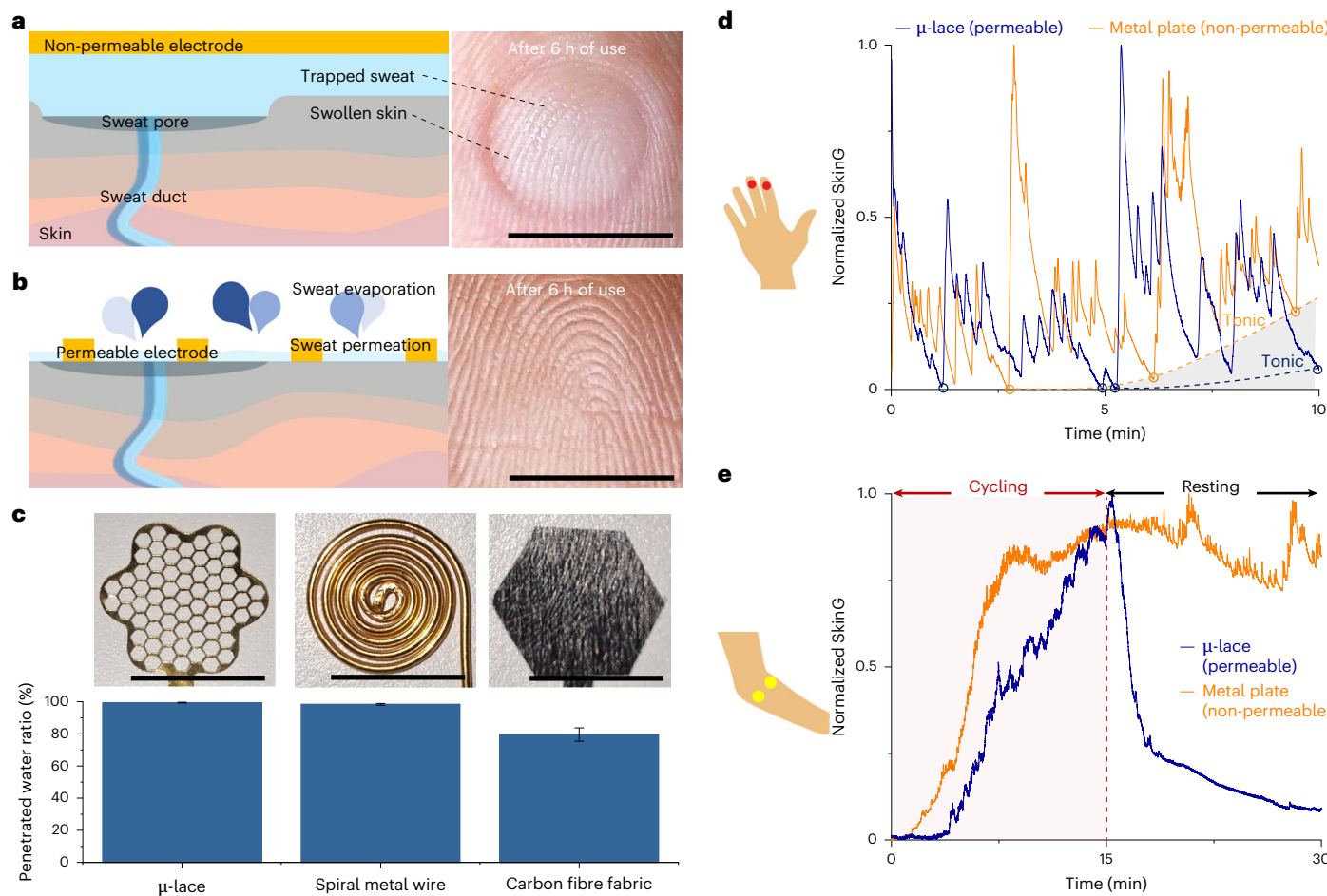


**Fig. 2 | Concepts and various kinds of permeable electrode for SkinG sensor.**

**a**, Schematic of the skin-electrode interface with a non-permeable electrode, along with the corresponding photograph of the fingertip after 6 h of use with a non-permeable metal plate electrode. Scale bar, 1 cm. **b**, Schematic of the skin-electrode interface with a permeable electrode, along with the corresponding photograph of the fingertip after 6 h of use with a permeable  $\mu$ -lace electrode.

Scale bar, 1 cm. **c**, Photographs of three types of permeable electrode ( $\mu$ -lace, spiral metal wire and carbon fibre fabric) and comparison of water permeability. Scale bar, 1 cm. **d**, SkinG variations on the fingertip at rest between permeable  $\mu$ -lace electrodes and non-permeable metal plate electrodes. **e**, SkinG recovery responses on the upper arm between permeable  $\mu$ -lace electrodes and non-permeable metal plate electrodes after 15 min of cycling on a stationary bike.

forehead<sup>8</sup> (Supplementary Note 3). By contrast, no SkinG changes are observed for mental stimuli on sites with lower sweat gland densities. When physical activity is conducted, all sites may show increments in SkinG because physical activities can activate the sweat glands for thermoregulation<sup>5,24</sup>, inducing high sweating. However, although sites with lower gland densities only show a cumulative tonic response, the high-density sites show both tonic and phasic responses with the same order of magnitude. We can discriminate between mental and physical activities by identifying the typical form of the signals from multisite measurements.

### Permeable electrodes for SkinG sensor

As schematically illustrated in Fig. 2a, a non-permeable electrode can trap sweat and induce swelling of the skin underneath the electrode on extended wear. After 6 h of use on the fingertip, the non-permeable plate metal electrode left a blanching mark on swollen skin, indicating that sweat was trapped underneath the electrode. By contrast, a permeable electrode enables the permeation of sweat through the holes of electrodes and the evaporation of sweat into the air, and the  $\mu$ -lace electrode did not leave any mark on the skin after the same period (Fig. 2b).

As electrodes for SkinG sensing, we introduce various kinds of water-permeable and conductive electrode (Fig. 2c), including  $\mu$ -lace electrodes, spiral metal wire electrodes and carbon fibre fabric electrodes. The penetrated water ratio is defined as the amount of water

that passed through the sample divided by the total amount of poured water (Methods) and measured for each electrode with three different designs, finding that  $\mu$ -lace and spiral wire present nearly complete water permeability and negligible water absorption, with 99.4% and 98.4% of penetrated water ratio, respectively. Although the carbon fibre fabric showed a moderate permeability of 89.6%, these fabric-based electrodes may have a specific use case because of their high wearability. Moreover, the penetrated water ratio by flowing water through the electrode at different flow rates was similarly high at different flow rates (Supplementary Fig. 6).

For direct and conformal contact to the skin,  $\mu$ -lace patterns were optimized further using computer-assisted laser cutting (Supplementary Fig. 7). We designed the pattern of close-packed hexagons with a spacing of 1.27 mm with three different lace widths of approximately 50  $\mu$ m, 100  $\mu$ m and 200  $\mu$ m (Supplementary Fig. 7a). The different laces showed permeability of 99.4%, 99.0% and 98.2%, respectively (Supplementary Fig. 7b). In particular, the  $\mu$ -lace electrodes are mechanically stretchable due to the structural design of the holes, thereby allowing for conformal contact with the skin. This enables low-resistance dry contacts without the need for gels. To evaluate the electromechanical properties of our  $\mu$ -lace electrodes, we compared electrical resistance as a function of stretching (Supplementary Fig. 7c,d). The  $\mu$ -lace electrodes show minimal resistance change up to 8% strain. This design, thus, has low sensitivity to motion artefacts. We confirmed that forearm

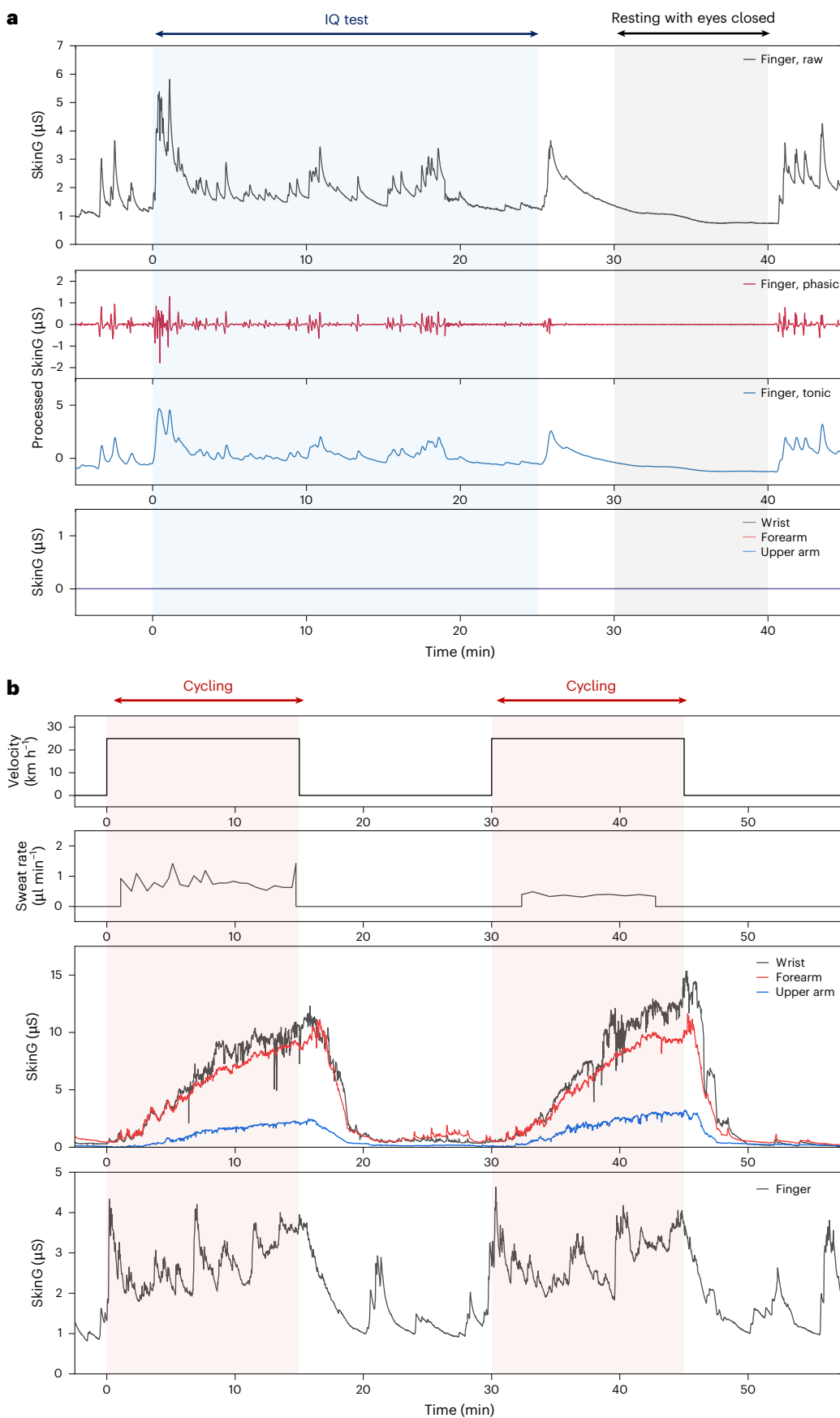


**Fig. 3 | Qualitative SkinG analysis of mental and physical activities on different body sites.** **a**, SkinG change profiles on four different sites (finger, wrist, forearm and upper arm) during psychological activities such as IQ tests and resting with eyes closed. **b**, SkinG change profiles on four different sites (finger, wrist, forearm and upper arm) during stationary cycling.

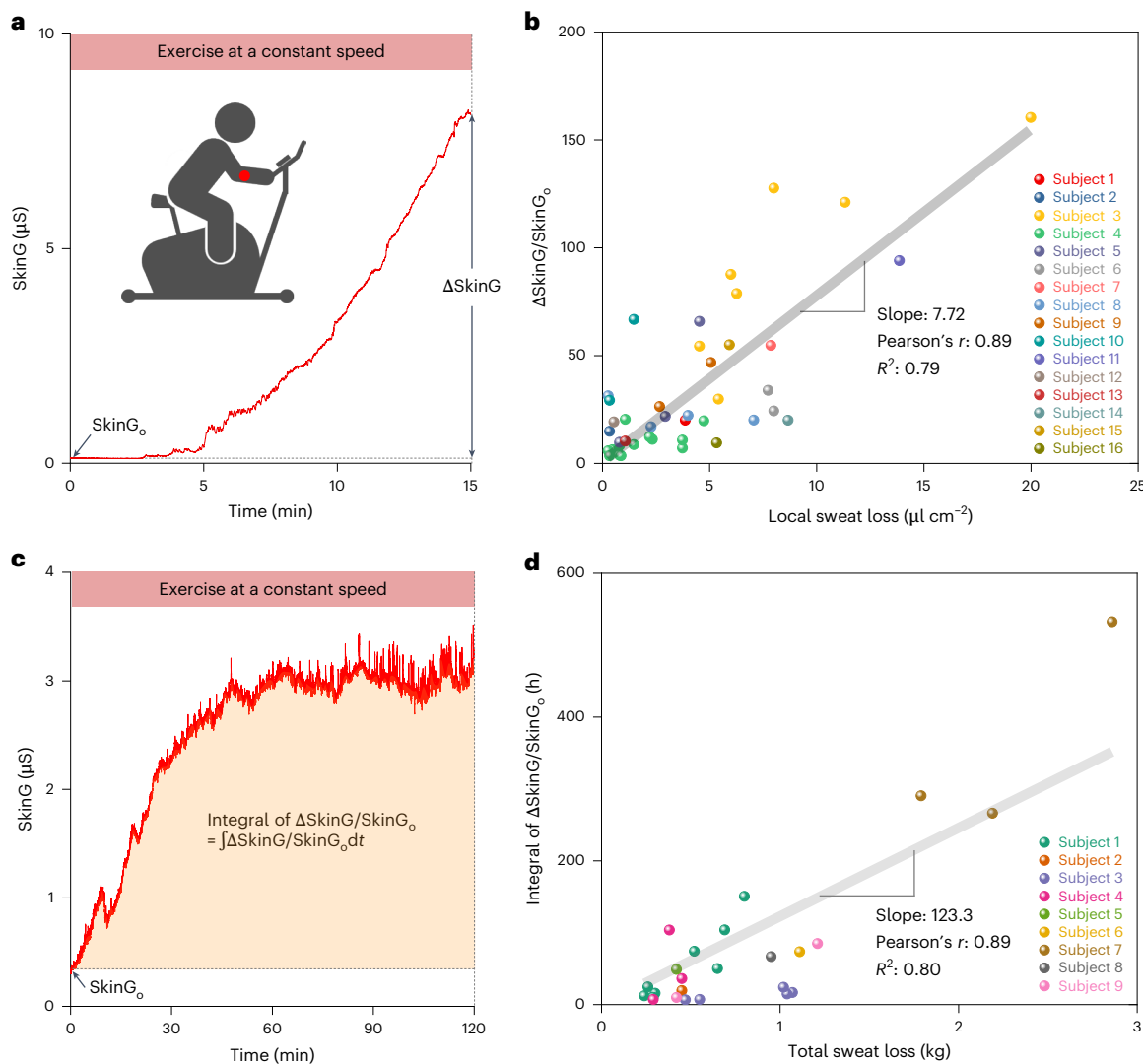


**Fig. 4 | On-body real-time participant study during stationary cycling for quantitative analysis.** **a**, Schematic of the test setup for participant study and SkinG change during 15-min exercise at a constant speed. **b**, Correlation between  $\Delta\text{SkinG}/\text{SkinG}_0$  and local sweat loss from 16 participants using a SkinG sensor

and a commercial sweat collector. **c**, SkinG change during 120-min exercise at a constant speed. **d**, Correlation between the integral of  $\Delta\text{SkinG}/\text{SkinG}_0$  and total sweat loss from nine participants using a SkinG sensor and measuring body weight change.

SkinG showed little changes due to movements inducing skin surface compression and tension (Supplementary Fig. 8). Additionally, no motion artefact was seen during running on the treadmill with aggressive arm movements (Supplementary Fig. 9).

The effect of the electrode's permeability on SkinG was evaluated on both finger (at rest) and upper arm (during and after exercise) using permeable  $\mu$ -lace and non-permeable metal plate electrodes. In Fig. 2d, a large increase (~25%) in the tonic response (that is, SkinG baseline) of the finger is observed after 10 min with metal sheet electrodes as the participant is at rest, corresponding to the accumulation of sweat under the electrodes. By contrast, a minimal change is observed in the tonic response for the  $\mu$ -lace electrodes. The effect of the electrodes' permeability was also examined on the upper arm during 15 min of cycling on a stationary bike (Fig. 2e). With non-permeable electrodes, we observe (1) early saturation of SkinG during physical activity and (2) less recovery after physical activity<sup>25</sup>. Specifically, the permeable  $\mu$ -lace electrodes showed over 90% recovery of SkinG after 15 min of resting, whereas the non-permeable metal plate electrodes showed no recovery. The same increasing tonic responses and less-recovering trends were confirmed using non-permeable standard commercial Ag/AgCl electrodes (Supplementary Fig. 10).

## Qualitative SkinG analysis by physical and mental activities

SkinG on the finger can be used for mental activity monitoring, whereas the wrist, forearm and upper arm can be used for physical activity monitoring. For multisite measurements to monitor both mental and physical activities, four permeable SkinG sensors were mounted on four different sites (finger, wrist, forearm and upper arm) on the participant with a microfluidic sweat rate sensor. To apply the mental stimulus, the participant conducted an IQ test for 25 min and subsequently rested with their eyes closed for 10 min (Fig. 3a). SkinG from the finger was processed with high-pass filtering to separate the phasic and tonic responses, as typically done in EDA analysis (Methods). Rested and peaceful mental states show sparse spikes on the finger SkinG, whereas nervous and irritated states from mental stimuli can fire frequent repetitive signals. Here no change in SkinG was observed on the wrist, forearm and upper arm during this mental activity.

A similar multisite measurement was performed to monitor physical activity during stationary cycling. Under a two-phase cycling activity with controlled pedalling resistance and fixed speed (Fig. 3b), the SkinG from the wrist, forearm and upper arm showed similar increasing trends, followed by fast recovery to the baseline during periods of rest.

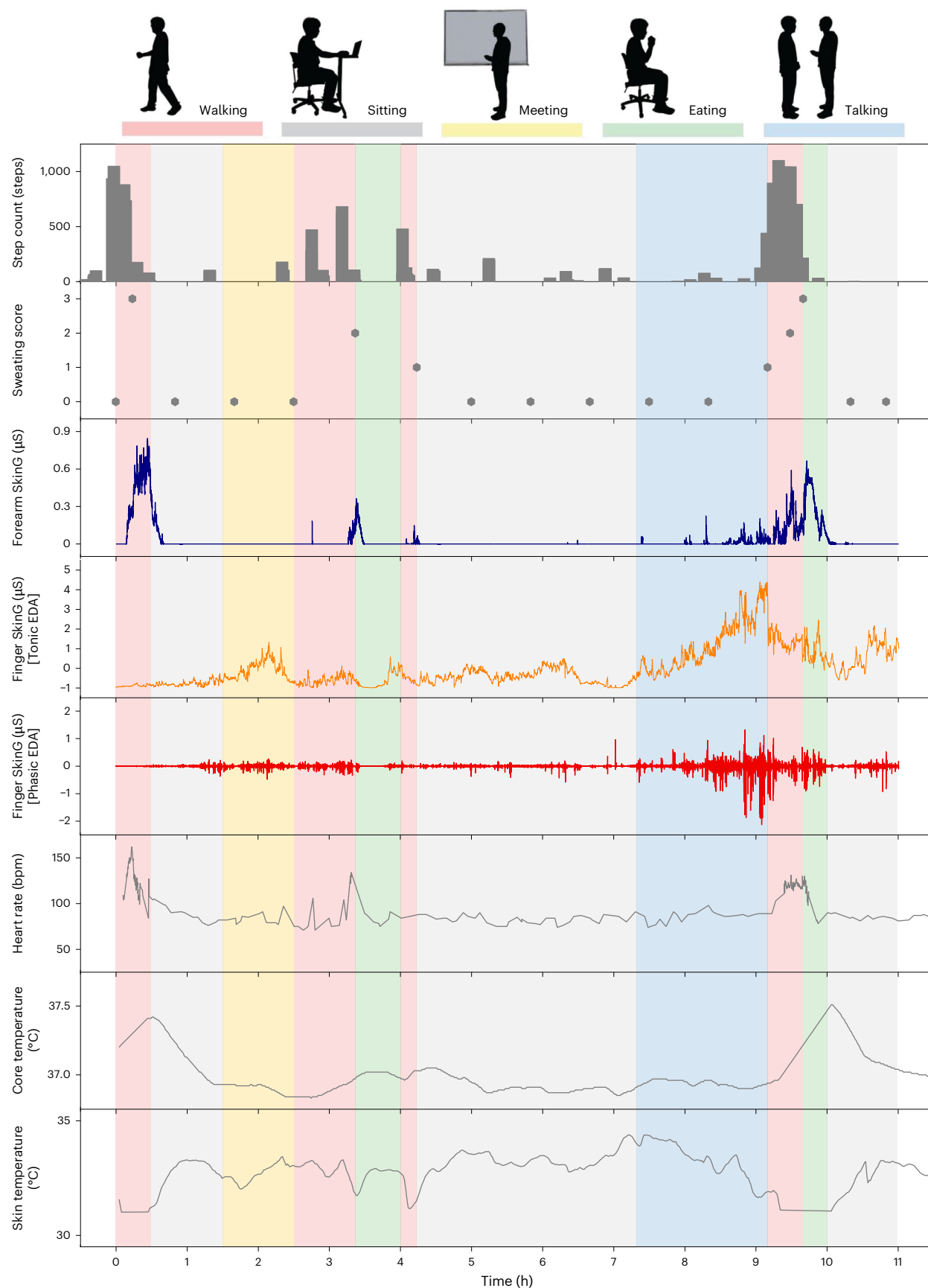


**Fig. 5 | Monitoring physical and mental activities with long-term use of SkinG sensor.** A participant wore two SkinG sensors on the forearm and fingers, an activity tracker on the wrist and a temperature sensor on the wrist during 11 h of daily activities (walking, sitting, meeting, eating and talking). Also, the participant qualitatively scored their sweat rate on a scale from 0 to 3.

Simultaneously, the sweat rate was measured on the forearm using a custom microfluidic channel device (Fig. 1a) for continuous qualitative SkinG analysis. On the finger, we observe both tonic and phasic responses during exercise, meaning that finger SkinG is reflective of both mental and physical activities. Since the SkinG values for the wrist, forearm and upper arm are only responsive to physical activity and the SkinG value for the fingertip is responsive to both physical and mental activities, the results suggest that we can distinguish between mental and physical activities using multisite measurements.

## Participant study for quantitative correlation between SkinG and skin hydration

To quantitatively correlate SkinG and sweat loss during exercise, we conducted a participant study measuring both SkinG and sweat secretion volume in localized areas. As shown in Fig. 4a, 16 participants exercised on the stationary bike at a constant speed for 15 min wearing the SkinG sensor on the forearm. Cycling speed on the stationary bike depended on the participant but was constant throughout each experiment. Simultaneously, local sweat loss was measured using a commercial Macrodust sweat collector. The effect of cycling speed on SkinG for fixed 15-min exercise was evaluated for the same participant (Supplementary Fig. 11). Both SkinG and sweat loss increase with the cycling speed. Note the sweat volume data could not be obtained at slower speeds of  $18 \text{ km h}^{-1}$  and  $19.5 \text{ km h}^{-1}$  due to the dead volume of the commercial Macrodust sweat collector, showing the clear advantage of the SkinG sensor for monitoring low sweat rates.

To calibrate for participant-specific differences in skin properties such as skin thickness or ease of sweat absorption, relative changes in SkinG ( $\Delta\text{SkinG}/\text{SkinG}_0$ ) were calculated by dividing the SkinG variation ( $\Delta\text{SkinG}$ ) by the baseline SkinG at rest ( $\text{SkinG}_0$ ), as shown in Supplementary Note 2. As shown in Fig. 4b and further detailed in Supplementary Table 2, a strong positive correlation is observed between the relative change in SkinG and local sweat loss with the Pearson correlation coefficient ( $r$ ) of 0.89 and the coefficient of determination ( $R^2$ ) of 0.79 for the linear fit. This positive relation indicates that SkinG values are proportional to the amount of sweat secreted and absorbed into the SC, which affects skin hydration.

Also, the relative change in SkinG can be used for the hydration assessment of exercising people by integrating its area (Fig. 4c). Nine participants cycled on the stationary bike at an approximately constant speed for a longer time (30 min to 2 h), and they weighed themselves without any clothes before and after exercise. By subtracting the weight after exercise from the weight before exercise, we could get the total sweat loss. In Fig. 4d, there is a positive correlation between the integral of the relative SkinG change and total sweat loss with  $r$  of 0.89 and  $R^2$  of 0.80 for the linear fit. Also, when the participants cycled for 2 h on a stationary bike, the approximately constant speed of cycling maintained their heart rate at a similar value (Supplementary Figs. 12–14). We could see three typical phases in SkinG over time: increasing, stable and decreasing. These may demonstrate the effect of current hydration status on the sweat rate, but further participant studies are needed.

## Long-term use of SkinG sensor for simultaneous monitoring of physical and mental activities

Next, we evaluate the long-term use of SkinG sensors with a wireless board. In Fig. 5, the participant wore two SkinG sensors on the finger and the forearm for over 11 h to continuously and selectively monitor mental and physical activities during a typical daily routine, including walking, sitting, meeting, eating, and talking indoors and outdoors. An activity tracker for steps and heart rate, skin and core temperature sensor, and self-assessed sweating scores were used simultaneously. Step count and sweating score from walking matched well with increasing forearm SkinG. In particular, the sensor does not show any drift in the baseline SkinG at rest with rapid recovery throughout the length of measurement without the accumulation of sweat on the skin, whereas a standard commercial

Ag/AgCl electrode shows fluctuating drift of the forearm SkinG after walking (Supplementary Fig. 15). The phasic SkinG data from the finger depict excitement and psychological stimuli during mental activities like meeting and talking. Furthermore, the finger SkinG measurements during sleeping demonstrate some association between frequencies of phasic spikes and sleep state (Supplementary Figs. 16–18). We believe that SkinG sensing enhances current wearable sensing platforms and has the potential to facilitate additional fundamental physiological studies.

## Conclusions

We have reported the development of a multimodal sweat-sensing platform to locally measure sweat loss with microfluidics and assess skin hydration levels with SkinG sensors. By using water-permeable  $\mu$ -lace electrodes, the drift in tonic response from sweat accumulation under the device is mitigated, allowing sweating events to be monitored under both low and high physical activity levels. We demonstrated the use of SkinG as a proxy for sweat rate. We find that the response to physical and mental stimuli depends on the skin site, thereby allowing for the selective monitoring of physical and mental activities with multisite SkinG measurements. Our multimodal sweat sensing system could provide an ideal platform for sweat secretion monitoring for physical and mental activities. Future work includes further calibration of the environmental and individual characteristic parameters, including humidity, temperature and skin thickness.

## Methods

### Fabrication of multimodal sweat sensors

Among the permeable electrodes, the stainless steel wire and copper wire were wound to form a spiral pattern for the spiral metal wire electrodes. To make copper chemically stable, we electroplated gold on the surface of the copper wire. The  $\mu$ -lace electrodes were laser patterned using a Trotec Speedy 400 laser running at 5–15% power, 0.3–0.5% speed and 60 kHz on 10- $\mu\text{m}$  polyethylene terephthalate with a titanium/gold thin film of 50/100 nm, respectively. Carbon fibre fabric was purchased from Technical Fibre Products. SkinG sensors were anchored on the skin with a self-adhesive bandage (BAND-AID, Johnson & Johnson) for stable contact (Supplementary Fig. 1). For integrated multimodal sweat sensors,  $\mu$ -lace electrodes were laminated on the inlet side of the microfluidic channel. A detailed description of the fabrication process of microfluidic channels was included in a previous study<sup>26</sup>.

### Water penetration test for permeability characterization

We conducted the water penetration test by pouring 1 g of water onto the sample suspended over a container and measuring the mass changes. After removing the sample, we determined the amount of water that passed through. Dividing this by the total amount of poured water, we calculated the penetrated water ratio depending on different flow rates.

### Printed circuit board for wireless SkinG sensor

SkinG at up to four skin sites was measured continuously via a custom printed circuit board implementing the standard exosomatic direct-current voltage method with wireless readout to a mobile application (Supplementary Figs. 19 and 20 and Supplementary Table 3). The electrical properties of skin can also be measured with an alternating-current excitation, but direct-current SkinG measurements are more established in the field and utilize simpler circuitry (Supplementary Note 2). A transimpedance amplifier is configured with an LTC2063 operational amplifier, applying a 0.8–1 V voltage between the on-skin electrodes and including a current-limiting resistor preventing the applied current from exceeding 100  $\mu\text{A}$ ; note that the limit of human perception is typically taken to be 1 mA (Supplementary Table 4). Each pair of electrodes is measured at 1 Hz with a 250-ms interval between sites. The resolution range is 0–32.7  $\mu\text{S}$ ; typical SkinG falls between 1  $\mu\text{S}$  and 20  $\mu\text{S}$  (Supplementary Table 5). Readings are

transmitted to a mobile phone via Bluetooth Low Energy for data monitoring and export. As shown in Supplementary Fig. 21, a phone application was developed for wireless data transfer and extraction.

### On-body qualitative analysis for mental and physical activities

We selected four sites to test various body sites (finger, wrist, forearm and upper arm), and simultaneously measured both SkinG and local sweat loss using permeable electrodes and a microfluidic device, respectively. The microfluidic device used for continuous sweat rate monitoring was from our previous work<sup>26</sup>. The parallel electrode pair in Fig. 1b is located below the microfluidic spacer and the capping layer. Sweat fills the microfluidic channel in a spiral path through the inlet (Fig. 1b, white dashed line). As sweat flows through the microfluidic channel, it connects the legs of two parallel electrodes, which increases the admittance in a stepwise fashion, allowing the location of the fluid front of the sweat to be determined. The sweat rate can be calculated based on the cross-sectional area of the microfluidic channel, the distance between the fingers of the electrode and the time changes between the steps in admittance. Additionally, participants attached a commercial activity tracker (Fitbit) and a body temperature sensor (CORE) to the skin for comparison. The recorded heart rate and skin temperature during the mental and physical activities are shown in Supplementary Figs. 22 and 23, respectively. Participants conducted an online IQ test (<https://www.mensa.org/public/mensa-iq-challenge>) as a mental activity and cycling on the stationary bike as a physical activity.

### On-body quantitative participant study for physical activity

For SkinG sensing, the participant wore a pair of spiral metal wire electrodes only on the right forearm. To quantize the local sweat amount, participants wore a commercial microfluidic sweat collector (Macroduct) on the left forearm. Participants rested in a temperature- and humidity-controlled laboratory for at least 10 min and attached the sensor before the experiment. The experiments were conducted during the day in an environment with a temperature of 20–25 °C and a humidity of 40–60% (Supplementary Fig. 24). The participants were guided to ride the stationary bike for 15 min at a comfortable speed. Tests on the same participants were conducted on different days, and only those who felt comfortable increased their speed. After 15 min of exercise, the participant rested for more than 5 min. Data analysis and visualization were conducted using Origin, including graph plotting, slope calculation, data averaging and extraction of relevant parameters.

### SkinG data processing

The phasic levels and tonic levels of the SkinG signals were deconvoluted using a signal filter. A low-pass filter with a 0.05-Hz cut-off frequency extracts the tonic level, whereas a high-pass filter with the same cut-off frequency yields the phasic level. In practice, the related deconvolution was done by using the NeuroKit2 (ref. 27) Python library. The library provides the ‘eda\_phasic()’ function, which, by default, applies signal filters with 0.05-Hz cut-off frequency to decompose EDA into phasic and tonic components. The related online documentation can be accessed through their official website at [https://neuropsychology.github.io/NeuroKit/examples/eda\\_peaks/eda\\_peaks.html#decompose-eda-into-phasic-and-tonic-components](https://neuropsychology.github.io/NeuroKit/examples/eda_peaks/eda_peaks.html#decompose-eda-into-phasic-and-tonic-components).

### Long-term use of SkinG sensor with various physiological sensors for daily activities monitoring

We selected the finger and forearm to mount the SkinG sensor. With permeable spiral metal wire electrodes, we simultaneously attached a commercial activity tracker (such as an Apple Watch or Fitbit) and a body temperature sensor (CORE) to the skin for comparison. The self-scored sweat rate was qualitatively assessed on a scale from 0 to 3. A sweat score of 0 corresponds to at-rest sweat rates, whereas a score of 3 corresponds to heavy sweating, similar to when the participant undergoes intense exercise.

### Reporting summary

Further information on research design is available in the Nature Portfolio Reporting Summary linked to this article.

### Data availability

The data that support the findings of this study are available from the corresponding author upon reasonable request.

### Code availability

The codes used for collecting data are available from the corresponding author upon reasonable request.

### References

- Ali, N., Tschenett, H. & Nater, U. M. in *Encyclopedia of Mental Health (Third Edition)* (eds Friedman, H. S. & Markey, C. H.) 221–231 (Academic Press, 2023).
- Fu, Q. & Levine, B. D. in *Handbook of Clinical Neurology Vol. 117* (eds Buijs, R. M. & Swaab, D. F.) 147–160 (Elsevier, 2013).
- Ates, H. C. et al. End-to-end design of wearable sensors. *Nat. Rev. Mater.* **7**, 887–907 (2022).
- Krittawong, C. et al. Integration of novel monitoring devices with machine learning technology for scalable cardiovascular management. *Nat. Rev. Cardiol.* **18**, 75–91 (2021).
- Yang, D. S., Ghaffari, R. & Rogers, J. A. Sweat as a diagnostic biofluid. *Science* **379**, 760–761 (2023).
- Bariya, M., Nyein, H. Y. Y. & Javey, A. Wearable sweat sensors. *Nat. Electron.* **1**, 160–171 (2018).
- Ho, A. V. T., Toska, K. & Wesche, J. Rapid, large, and synchronous sweat and cardiovascular responses upon minor stimuli in healthy subjects. Dynamics and reproducibility. *Front. Neurol.* **11**, 51 (2020).
- Boucsein, W. *Electrodermal Activity* (Springer Science & Business Media, 2012).
- Harker, M. Psychological sweating: a systematic review focused on aetiology and cutaneous response. *Skin Pharmacol. Physiol.* **26**, 92–100 (2013).
- van Dooren, M., de Vries, J. J. G. & Janssen, J. H. Emotional sweating across the body: comparing 16 different skin conductance measurement locations. *Physiol. Behav.* **106**, 298–304 (2012).
- Regalia, G., Resnati, D. & Tognetti, S. in *Encyclopedia of Sensors and Biosensors (First Edition)* (ed. Narayan, R.) 1–20 (Elsevier, 2023).
- Jang, H. et al. Graphene e-tattoos for unobstructive ambulatory electrodermal activity sensing on the palm enabled by heterogeneous serpentine ribbons. *Nat. Commun.* **13**, 6604 (2022).
- Morin, M. et al. Skin hydration dynamics investigated by electrical impedance techniques in vivo and in vitro. *Sci. Rep.* **10**, 17218 (2020).
- Yao, S. et al. A wearable hydration sensor with conformal nanowire electrodes. *Adv. Healthcare Mater.* **6**, 1601159 (2017).
- Xu, C. et al. A physicochemical-sensing electronic skin for stress response monitoring. *Nat. Electron.* **7**, 168–179 (2024).
- Posada-Quintero, H. F. et al. Time-varying analysis of electrodermal activity during exercise. *PLoS ONE* **13**, e0198328 (2018).
- Pontarollo, F., Rapacioli, G. & Bellavite, P. Increase of electrodermal activity of heart meridian during physical exercise: the significance of electrical values in acupuncture and diagnostic importance. *Complement. Ther. Clin. Pract.* **16**, 149–153 (2010).
- Boettger, S. et al. Heart rate variability, QT variability, and electrodermal activity during exercise. *Med. Sci. Sports Exerc.* **42**, 443–448 (2010).

19. Kim, H. et al. Fully integrated, stretchable, wireless skin-conformal bioelectronics for continuous stress monitoring in daily life. *Adv. Sci.* **7**, 2000810 (2020).
20. Xu, Y. et al. In-ear integrated sensor array for the continuous monitoring of brain activity and of lactate in sweat. *Nat. Biomed. Eng.* **7**, 1307–1320 (2023).
21. Zhang, B. et al. A three-dimensional liquid diode for soft, integrated permeable electronics. *Nature* **628**, 84–92 (2024).
22. Gidado, I. M., Qassem, M., Triantis, I. F. & Kyriacou, P. A. Review of advances in the measurement of skin hydration based on sensing of optical and electrical tissue properties. *Sensors* **22**, 7151 (2022).
23. Taylor, N. A. S. & Machado-Moreira, C. A. Regional variations in transepidermal water loss, eccrine sweat gland density, sweat secretion rates and electrolyte composition in resting and exercising humans. *Extrem. Physiol. Med.* **2**, 4 (2013).
24. Nyein, H. Y. Y. et al. Regional and correlative sweat analysis using high-throughput microfluidic sensing patches toward decoding sweat. *Sci. Adv.* **5**, eaaw9906 (2019).
25. Subramanian, S., Barbieri, R. & Brown, E. N. Point process temporal structure characterizes electrodermal activity. *Proc. Natl. Acad. Sci. USA* **117**, 26422–26428 (2020).
26. Dautta, M. et al. Tape-free, digital wearable band for exercise sweat rate monitoring. *Adv. Mater. Technol.* **8**, 2201187 (2023).
27. Makowski, D. et al. NeuroKit2: a Python toolbox for neurophysiological signal processing. *Behav. Res.* **53**, 1689–1696 (2021).

## Acknowledgements

On-body human trials were carried out at the University of California, Berkeley, in compliance with the human research protocol (CPHS 2014-08-6636) approved by the Berkeley Institutional Review Board (IRB). Informed consent was obtained from the participants before enrolment in the study. This work was partially supported by Samsung Electronics Company, Ltd, Berkeley Sensors and Actuators Center (BSAC), and the Bakar Fellowship. Part of the sensor fabrication was performed in the Electronic Materials (E-MAT) laboratory funded by the US Department of Energy, Office of Science, Office of Basic Energy Sciences, Materials Sciences and Engineering Division, under contract no. DE-AC02-05Ch11231 (Electronic Materials program). The work at VTT was funded by the Academy of Finland (grant agreement no. 351282). Technical contribution from H. Sääskilahti and J. Rekilä

is gratefully acknowledged. N.D. acknowledges support from the National Defense Science & Engineering Graduate (NDSEG) Fellowship Program.

## Author contributions

S.-R.K., Y.Z., N.D. and A.J. conceived the idea and designed the experiments. S.-R.K., Y.Z. and N.D. carried out the experiments with assistance from S.B. N.D. developed the printed circuit board. L.G., E.H. and J.H. contributed to the fabrication of microfluidics with printed electrodes. S.-R.K., Y.Z., N.D., S.B. and A.J. contributed to the data analysis and interpretation. All authors discussed the results and revised the manuscript.

## Competing interests

The authors declare no competing interests.

## Additional information

**Supplementary information** The online version contains supplementary material available at <https://doi.org/10.1038/s41928-025-01365-7>.

**Correspondence and requests for materials** should be addressed to Ali Javey.

**Peer review information** *Nature Electronics* thanks Sheng Xu and the other, anonymous, reviewer(s) for their contribution to the peer review of this work.

**Reprints and permissions information** is available at [www.nature.com/reprints](http://www.nature.com/reprints).

**Publisher's note** Springer Nature remains neutral with regard to jurisdictional claims in published maps and institutional affiliations.

Springer Nature or its licensor (e.g. a society or other partner) holds exclusive rights to this article under a publishing agreement with the author(s) or other rightsholder(s); author self-archiving of the accepted manuscript version of this article is solely governed by the terms of such publishing agreement and applicable law.

© The Author(s), under exclusive licence to Springer Nature Limited 2025

# Electrodermal activity as a proxy for sweat rate monitoring during physical and mental activities

---

In the format provided by the  
authors and unedited

## Table of Contents

Supplementary Note 1 | Comparison of studies measuring physical activity using SkinG.

Supplementary Note 2 | Electrical model of skin hydration and the baseline calibration process.

Supplementary Note 3 | Different SkinG responses from different body locations.

Supplementary Figure 1 | Anchoring permeable electrodes on the skin using permeable self-adhesive bandage.

Supplementary Figure 2 | The effect of ionic conductivity of sweat on SkinG.

Supplementary Figure 3 | Ambient temperature, heart rate, skin temperature, and SkinG change profiles on the forearm during stationary cycling after moving to the gym.

Supplementary Figure 4 | SkinG variations between permeable  $\mu$ -lace electrodes and non-permeable metal plate electrodes on different sites at rest.

Supplementary Figure 5 | SkinG variations between permeable  $\mu$ -lace electrodes and non-permeable metal plate electrodes on different sites when the skin was wet.

Supplementary Figure 6 | Flowing water through u-lace, spiral metal wire, and carbon fiber fabric.

Supplementary Figure 7 |  $\mu$ -lace electrodes design.

Supplementary Figure 8 | Forearm SkinG changes depending on the strain applied to the skin due to compression / tension movements.

Supplementary Figure 9 | Heart rate, skin temperature, SkinG changes during running on the treadmill.

Supplementary Figure 10 | SkinG variations using standard commercial Ag/AgCl electrodes.

Figure 11 | SkinG changes of the same subject with increasing bike speed.

Supplementary Figure 12 | Heart rate, skin temperature, and forearm SkinG profiles during 2 hours of stationary cycling: SkinG with increasing phase over time.

Supplementary Figure 13 | Heart rate, skin temperature, and forearm SkinG profiles during 2 hours of stationary cycling: SkinG with stable phase over time.

Supplementary Figure 14 | Heart rate, skin temperature, and typical forearm SkinG profiles during 2 hours of stationary cycling: SkinG with decreasing phase over time.

Supplementary Figure 15 | Long time monitoring of SkinG using standard commercial Ag/AgCl electrodes.

Supplementary Figure 16 | Representative phasic EDA waveform from the finger during sleeping.

Supplementary Figure 17 | Sleep status, heart rate, skin temperature, and phasic EDA from finger SkinG data during sleeping.

Supplementary Figure 18 | Frequency of phasic spikes from finger SkinG recorded during 12 nights of sleep in one subject.

Supplementary Figure 19 | Photograph of integrated SkinG multiplexed sensing system.

Supplementary Figure 20 | Design of SkinG printed circuit board for multiplexed wireless sensing.

Supplementary Figure 21 | The custom iOS mobile application for data display and export.

Supplementary Figure 22 | Heart rate and skin temperature changes during mental activities compared with phasic EDA from the finger SkinG.

Supplementary Figure 23 | Heart rate and skin temperature changes during physical activities compared with the forearm SkinG.

Supplementary Figure 24 | Ambient temperature and relative humidity on weekdays for 5 weeks in controlled laboratory with ventilation.

Supplementary Table 1 | Comparison of studies measuring physical activity using SkinG.

Supplementary Table 2 | 43 data points in Figure 4b for calculating confidence interval.

Supplementary Table 3 | SkinG board measurement characteristics.

Supplementary Table 4 | SkinG board safety.

Supplementary Table 5 | SkinG board measurement range.

## **Supplementary Note 1 | Comparison of studies measuring physical activity using SkinG.**

In Supplementary Table 1, we compared studies measuring physical activity using SkinG (or electrodermal activity, galvanic skin response). When the electrodes were attached to a finger, which is known to be useful for measuring mental activity, both tonic and phasic responses were present, so responses were checked by averaging, but baseline recovery was not always observed (References no. 16-18). Because there are limitations such as interference with daily activities and signal distortion when worn on the hand, others have attempted to use electrodes on the wrist or shoulder (References no. 15, 19). Instead of focusing on the tonic response from exercise, they focused on analyzing the phasic response to stress from physical activity, and also could not confirm baseline recovery. Another study used permeable electrodes on the palm in the form of serpentine ribbons, and the baseline recovery of the tonic response could be confirmed through a graph, but they also only analyzed the phasic response (References no. 12). In this study, we demonstrated simple and robust usage of SkinG with permeable electrodes for physical activity monitoring in various body positions.

## **Supplementary Note 2 | Electrical model of skin hydration and the baseline calibration process.**

The electrical properties of skin can be measured with either a DC excitation or an AC excitation. The resisting property to the electric flow is called electrical resistance ( $= 1 / \text{conductance}$ ) for DC measurement and electrical impedance ( $= 1 / \text{admittance}$ ) for AC measurement. The electrical impedance includes the values of the electrical resistance, the inductive reactance ( $= 2\pi \cdot \text{frequency} \cdot \text{inductance}$ ), and the capacitive reactance ( $= 1 / (2\pi \cdot \text{frequency} \cdot \text{capacitance})$ ), and depends on the AC input frequency. Since DC circuits have no frequency dependency, we only need to consider the skin's resistance and can ignore its reactance for our measurements of skin conductance. In addition, when analyzing the electrical characteristics of the skin using AC, the depth of the measured skin depends on the frequency, which has the disadvantage of making it difficult to measure the hydration of only the stratum corneum layer. Moreover, there is the possibility of signal interferences with the biopotential such as EMG.

With DC measurement, SkinG can be electrically modeled as

$$\text{SkinG} = 1 / (2 \cdot R_{sc}) = (1 / 2) \cdot \sigma_{max} \cdot A / t \cdot H$$

, where  $\sigma_{max}$  is the skin conductivity when the skin is saturated with sweat, A is the contacting area of electrodes, t is the skin thickness, and H is the skin hydration level ( $0 \leq H \leq 1$ ). To get the accurate H value from SkinG directly, the effect of individual subject's properties (such as ion concentration of the sweat, skin thickness, and skin tissue density) and other environmental factors (such as ambient temperature and ambient humidity) should be considered. Without the information of variable parameters, we can simply calculate  $2 \cdot \text{SkinG} / \text{SkinG}_{max}$ , where the  $\text{SkinG}_{max}$  is the SkinG when the skin is fully saturated with sweat ( $\text{SkinG}_{max} = \sigma_{max} \cdot A / t$ ), for the H value. However, since the time it takes for the skin

to become saturated by the sweat varies from subject to subject which was not practical, we decided to divide current SkinG ( $\text{SkinG}_{\text{current}}$ ) by initial SkinG ( $\text{SkinG}_{\text{initial}}$ ) to eliminate all the other variable parameters except for the ratio between current H ( $H_{\text{current}}$ ) and initial H ( $H_{\text{initial}}$ ). Moreover, to achieve a similar  $H_{\text{initial}}$  as controlled as possible, we had the subject rest in a temperature- and humidity-controlled laboratory for at least 10 minutes while attaching the sensor before the experiment.

Because our calibration process is still based on our assumptions such that the thickness of the skin or ion concentration of secreted sweat is constant over time, we acknowledge that some errors come about. However, our calibration is a good starting point that we can calculate the approximated correlation. Once we identify the influence of other variables, we can integrate them with sensors that can compensate for them and obtain more accurate correlations.

As shown in Supplementary Fig. 2, the effect of the ionic conductivity of sweat on SkinG was studied. 8 subjects exercised for 15 minutes and we collected their sweat. The conductivity of the collected sweat samples was measured, from which we extracted the ionic strength. We do not see a correlation between SkinG and sweat conductivity when not accounting for sweat rate (Supplementary Fig. 2c and d). On the other hand, as shown in Fig. 4b and d, there is a clear correlation between sweat rate (total sweat volume loss) and the SkinG (integral of SkinG), without calibration for sweat conductivity and despite the fact that different subjects used in our study had different sweat conductivity values. The effect of sweat ion concentration on SkinG is shown to be secondary, at most, from the subject studies.

Also, we carried out a cycling experiment at indoor 2 (hot and humid gym), after moving from indoor 1 (cool and dry lab) to indoor 2 (hot and humid gym) through outdoor (hot and dry) (Supplementary Fig. 3). It was confirmed that the SkinG increased significantly greater

during physical activity than by the environment. However additional detailed experiments must be conducted to compare the degree of response.

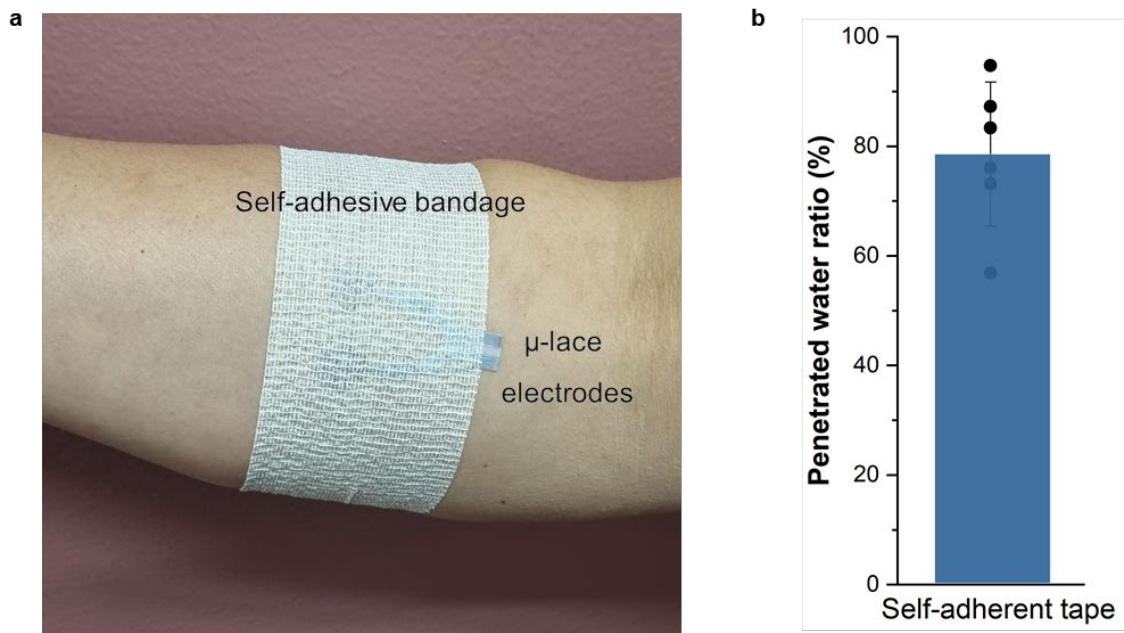
### **Supplementary Note 3 | Different SkinG responses from different body locations.**

Because the phasic EDA signals represent the filling and releasing of sweat glands, the number of sweat glands terminating at sweat pores in contact with the measurement electrodes directly affects both the frequency and the amplitude of the phasic EDA signal. So some sites with a lower density of sweat glands are not adequate for detecting electrical signals, even if psychological activities stimulate most of the sweat glands in that area via the sympathetic nervous system. Similarly, the smaller contact area of the permeable electrodes results in a lower initial SkinG value than commercial non-permeable electrodes. Also, the sweat exposed to the air through the holes of the permeable electrodes rapidly evaporates, which is insufficient to hydrate the skin at rest.

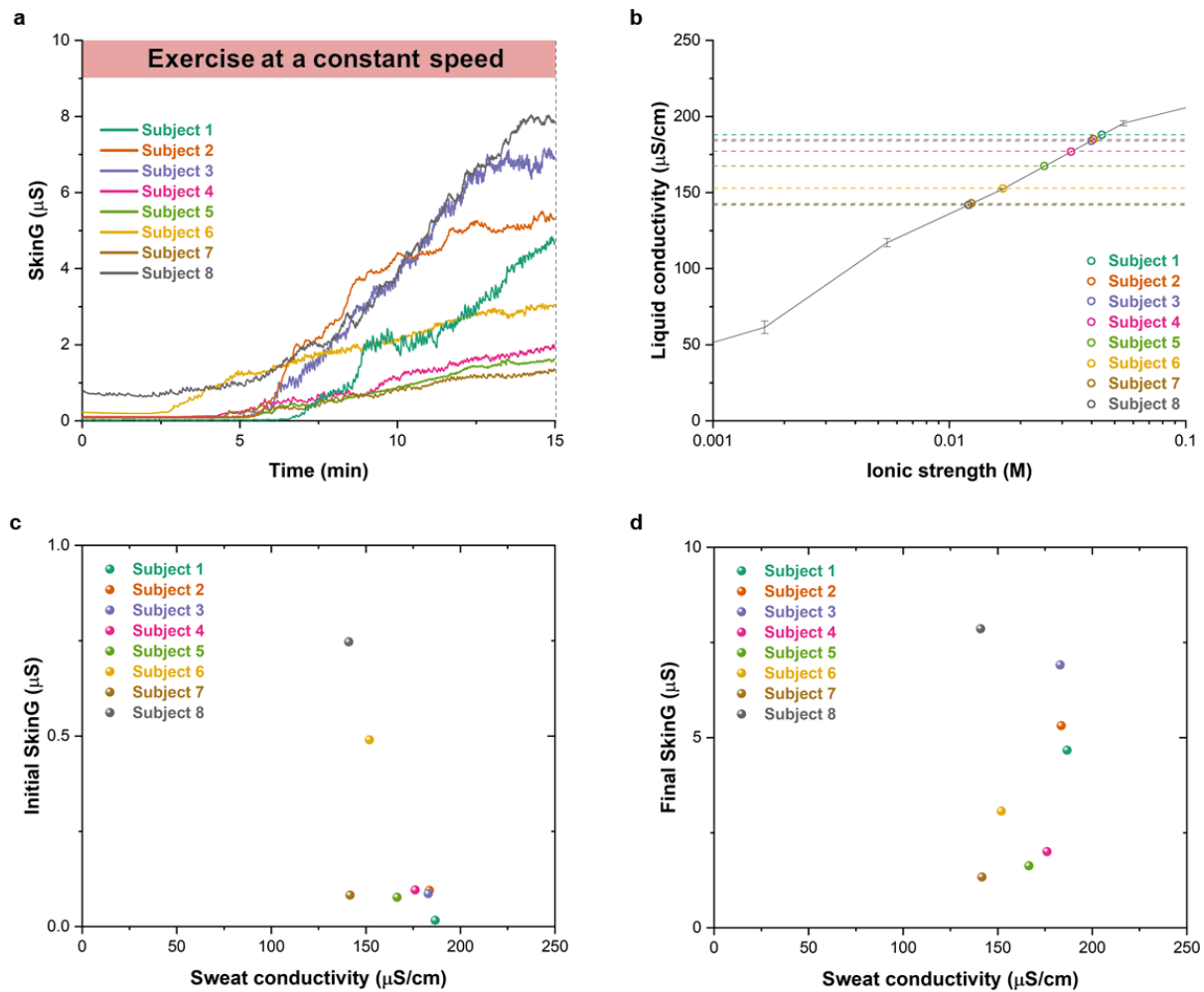
The hands, feet, and forehead are known to have a high density of sweat glands. As in Supplementary Fig. 4, we have tried to measure SkinG on three sites with high sweat gland density (toe, wrist, and forehead) and one site with low sweat gland density (forearm) using both permeable spiral metal wire and non-permeable metal plate. Subjects were resting, so their skin was dry. With the non-permeable metal plate electrodes, SkinG from the toe and forehead showed higher initial baseline values than the wrist and forearm. While the toe SkinG showed phasic responses, the forehead SkinG kept increasing for 10 minutes after putting the sensor on without saturating. With the permeable metal wire electrodes, we could see spikes from the sites with high sweat gland density, but it was hard to see even small spikes from the forearm. It seemed difficult to see a phasic response in the skin with a low density of sweat glands.

However, all sweat glands can secrete sweat even at rest. To confirm this, we also tried to measure SkinG of the hydrated skin on the wrist, forehead, and forearm, where it was hard to see the phasic EDA signals when dry (Supplementary Fig. 5). We could see higher baseline

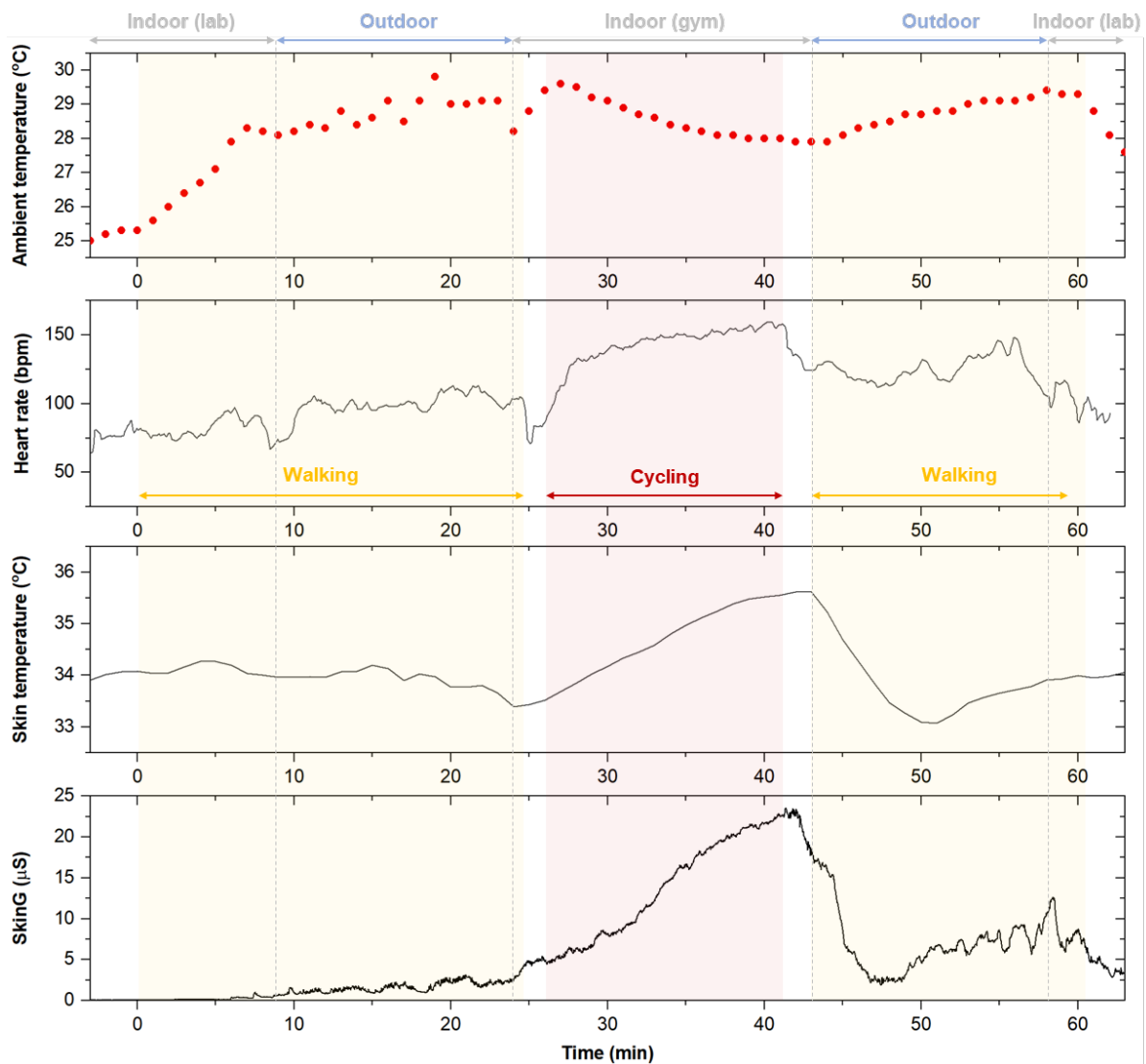
SkinG values. With the non-permeable metal plate electrodes, SkinG from wrist and forehead showed phasic responses. It was interesting that we could see phasic responses even on the forearm with a lower density of the sweat gland when the skin was wet. This indicates that non-permeable electrodes can capture phasic responses by trapping sweat and fully hydrating the skin underneath. On the forehead, we saw only a slightly increasing trend without the phasic spikes, even though the baseline SkinG value of wet skin was twice as high as the dry state. This may be due to the insufficiently moisturized stratum corneum, or small phasic spike sensitivity due to the high baseline.



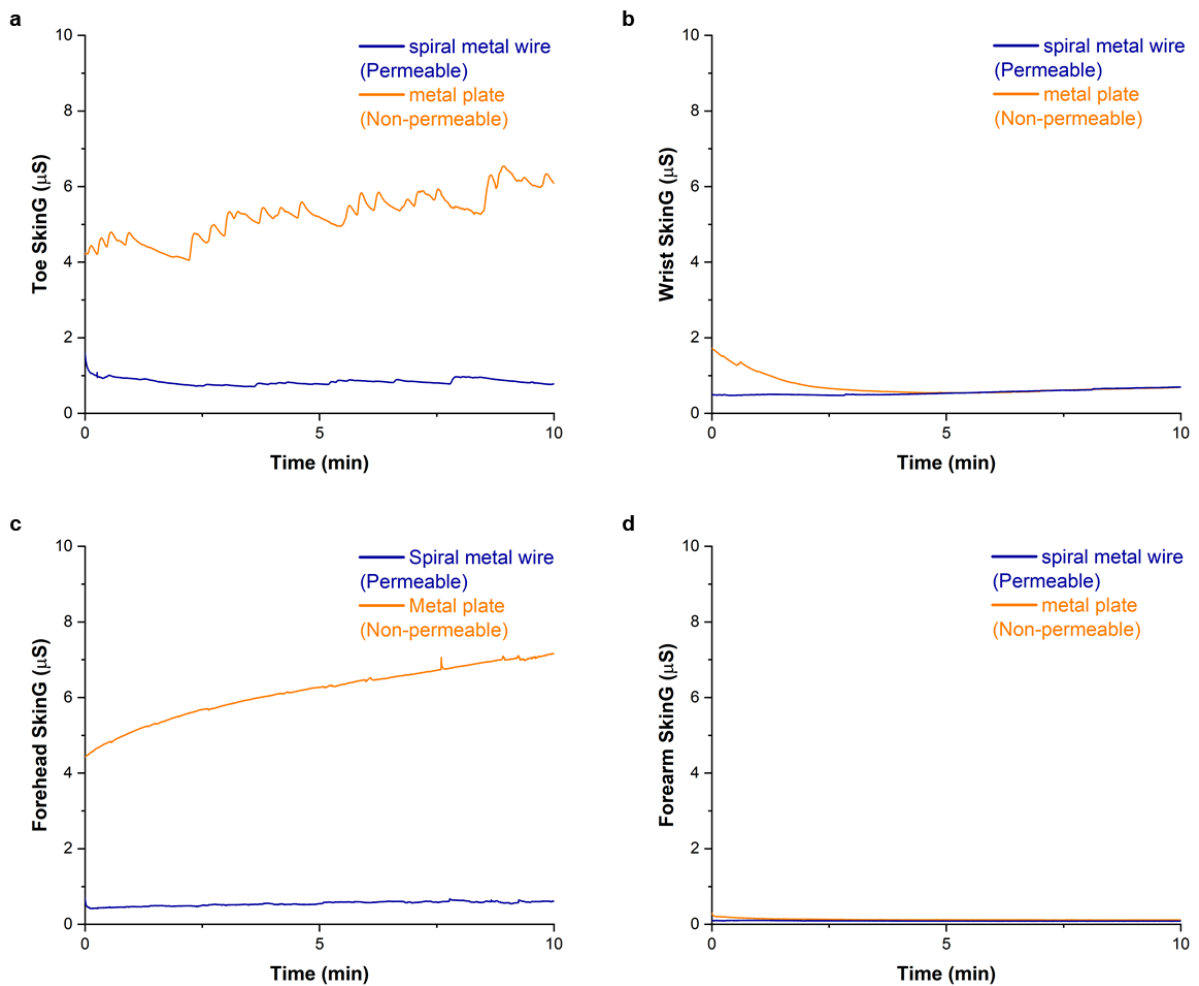
**Supplementary Figure 1 | Anchoring permeable electrodes on the skin using permeable self-adhesive bandage.** **a**, Photograph of permeable  $\mu$ -lace electrodes on the skin anchored by commercially available self-adhesive bandage (Band-Aid). **b**, Penetrated water ratio of the self-adhesive bandage.



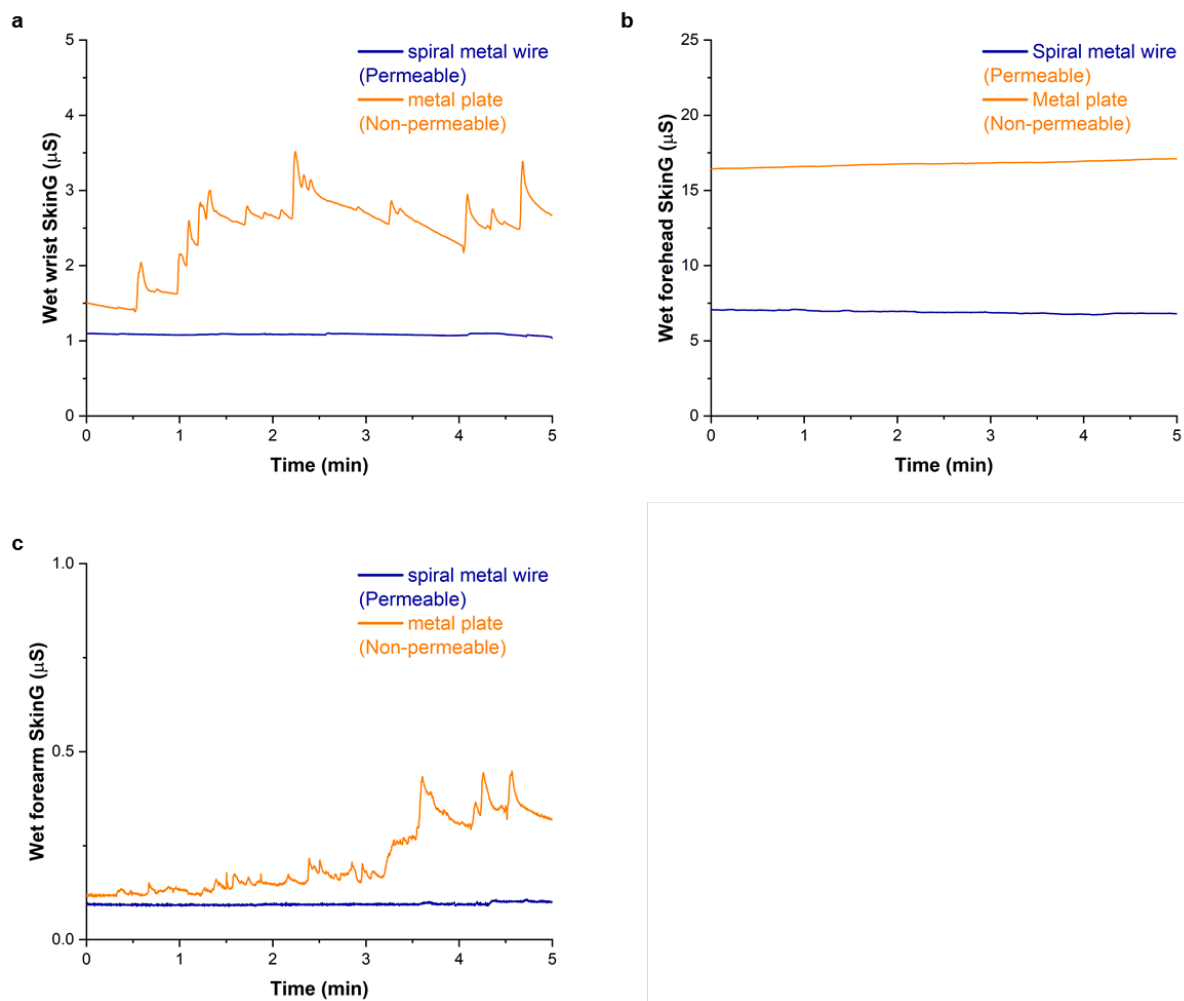
**Supplementary Figure 2 | The effect of ionic conductivity of sweat on SkinG.** **a**, SkinG changes on the forearm from the 8 subjects during 15 minutes of cycling a stationary bike. Initial and final SkinG are the SkinG at times 0 and 15 minutes, respectively. **b**, Measured sweat conductivity of 8 subjects was plotted with the conductivity of PBS with different ionic strength. **c**, Correlation between the sweat conductivity and the initial SkinG from 8 subjects (no positive correlation). **d**, Correlation between the sweat conductivity and the final SkinG from 8 subjects (no positive correlation).



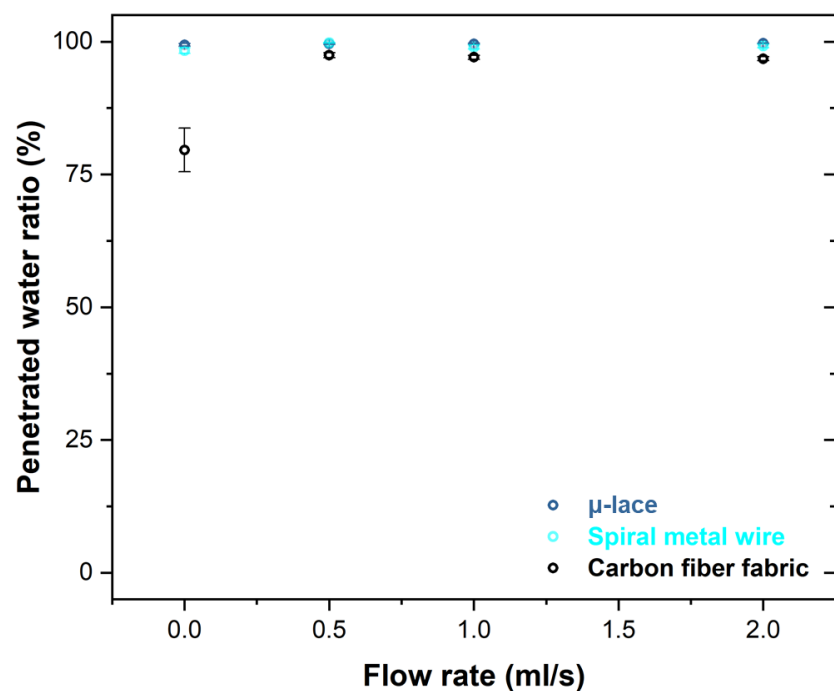
**Supplementary Figure 3 | Ambient temperature, heart rate, skin temperature, and SkinG change profiles on the forearm during stationary cycling after moving to the gym.**



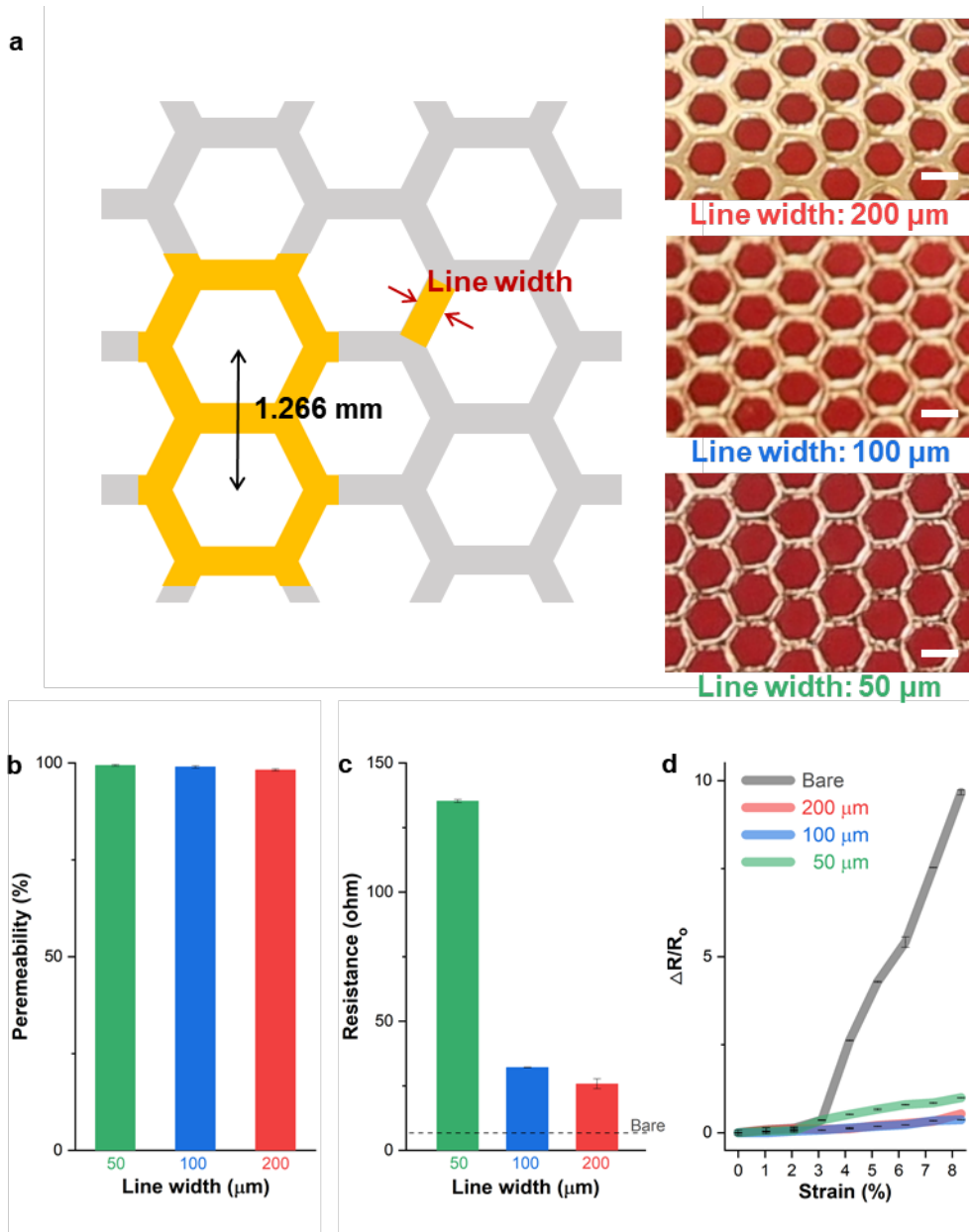
**Supplementary Figure 4 | SkinG variations between permeable  $\mu$ -lace electrodes and non-permeable metal plate electrodes on different sites at rest. (a: toe, b: wrist, c: forehead, d: forearm)**



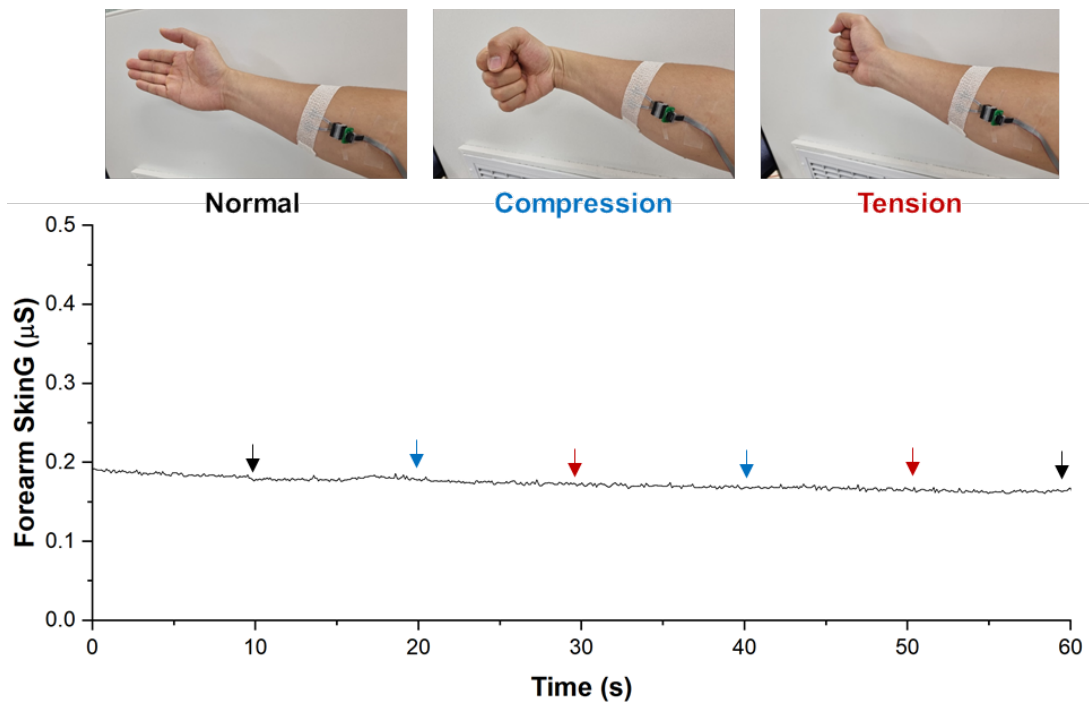
**Supplementary Figure 5 | SkinG variations between permeable  $\mu$ -lace electrodes and non-permeable metal plate electrodes on different sites when the skin was wet. (a: wrist, b: forehead, c: forearm)**



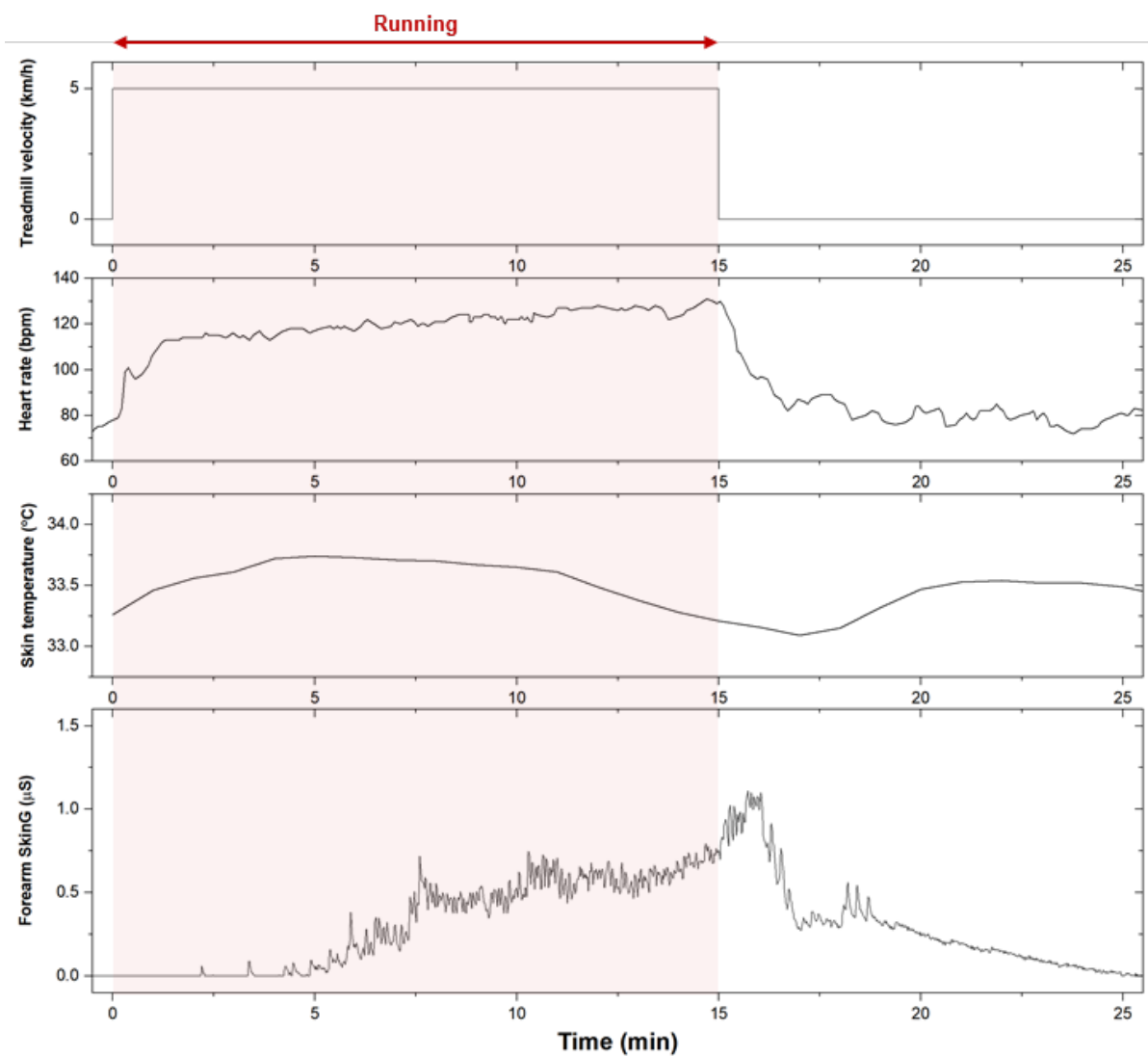
**Supplementary Figure 6 | Flowing water through u-lace, spiral metal wire, and carbon fiber fabric.** Penetrated water ratio increased over 99.5%, 99%, and 96.5%, respectively.



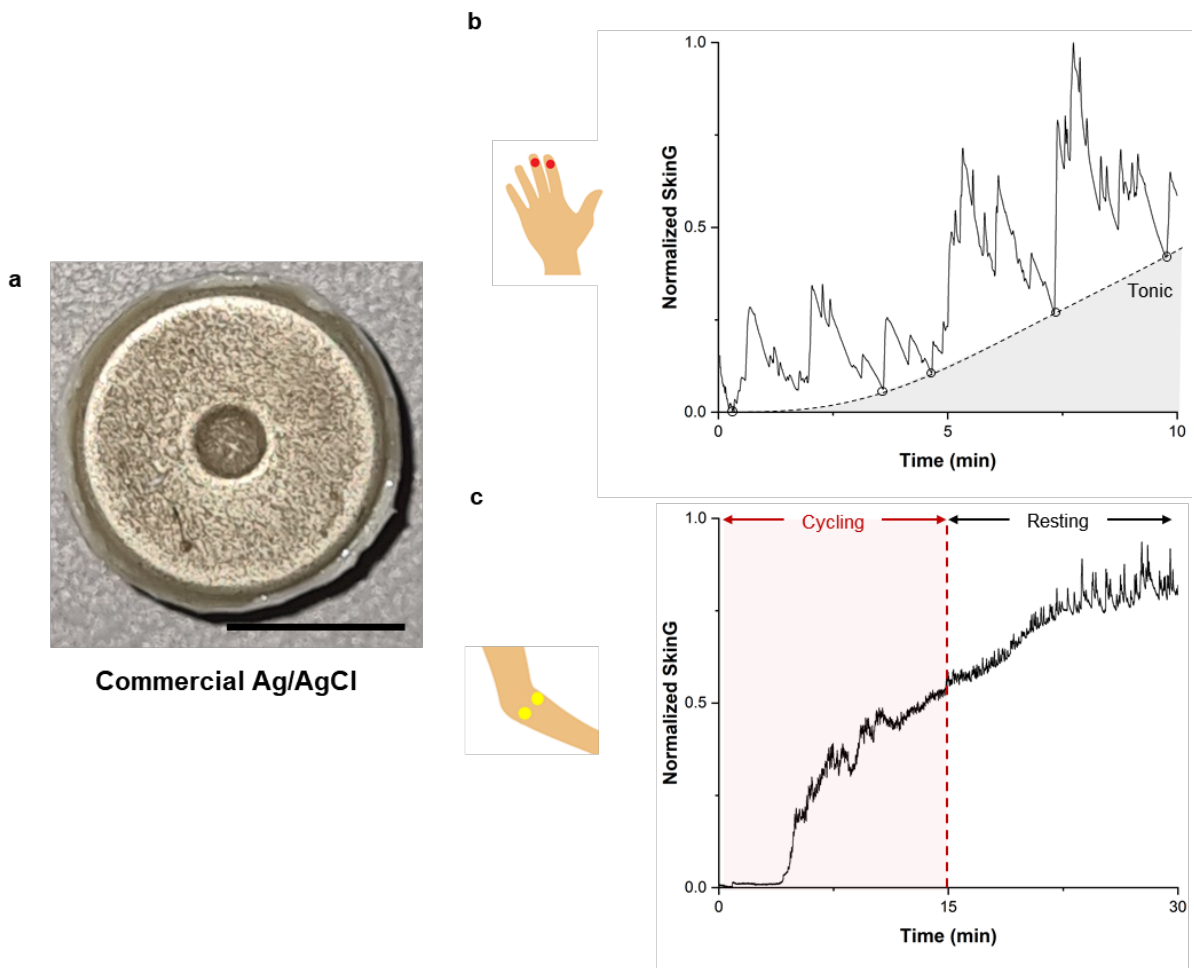
**Supplementary Figure 7 |  $\mu$ -lace electrodes design.** **a**, Schematic pattern of  $\mu$ -lace electrodes, along with photographs of  $\mu$ -lace electrodes with three different lace widths (50, 100, and 200  $\mu\text{m}$ ). (Scale bar, 1 mm) **b-d**, Comparison among three  $\mu$ -lace patterns of **(b)** water permeability, **(c)** electrical resistance of 12 mm  $\times$  55 mm electrodes, and **(d)** relative change of the resistance ( $\Delta R/R_o$ ) under stretching.



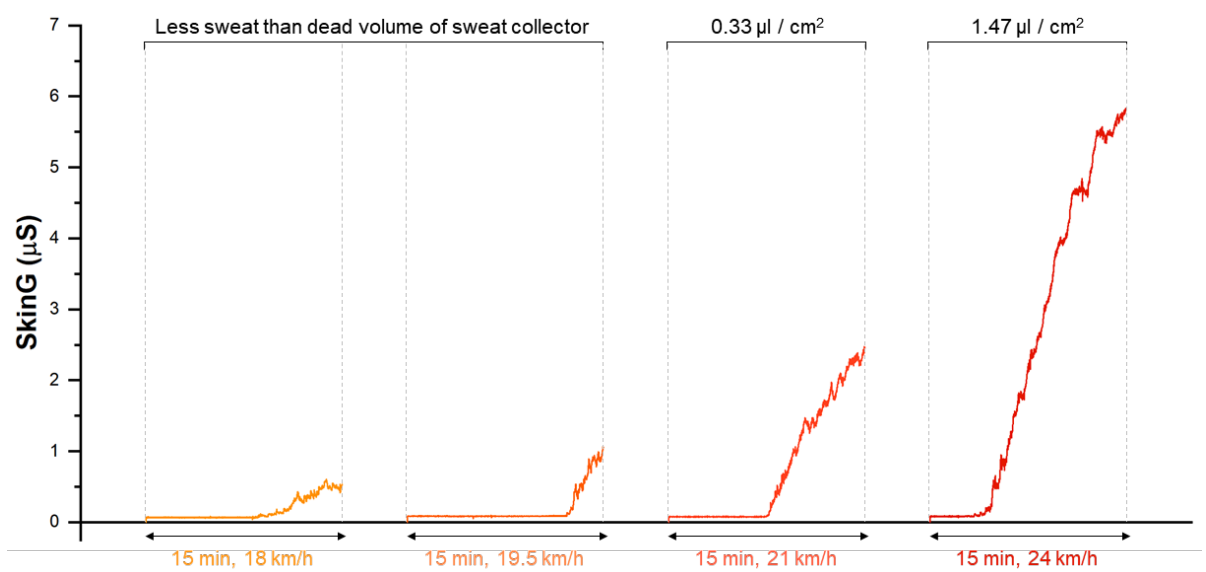
**Supplementary Figure 8 | Forearm SkinG changes depending on the strain applied to the skin due to compression / tension movements.** Putting  $\mu$ -lace electrodes on the curvilinear skin causes small bending deformation because they are thin films of about 10  $\mu$ m. Delamination does not occur because the sensor is tightly fixed using a permeable and stretchable self-adhesive bandage.



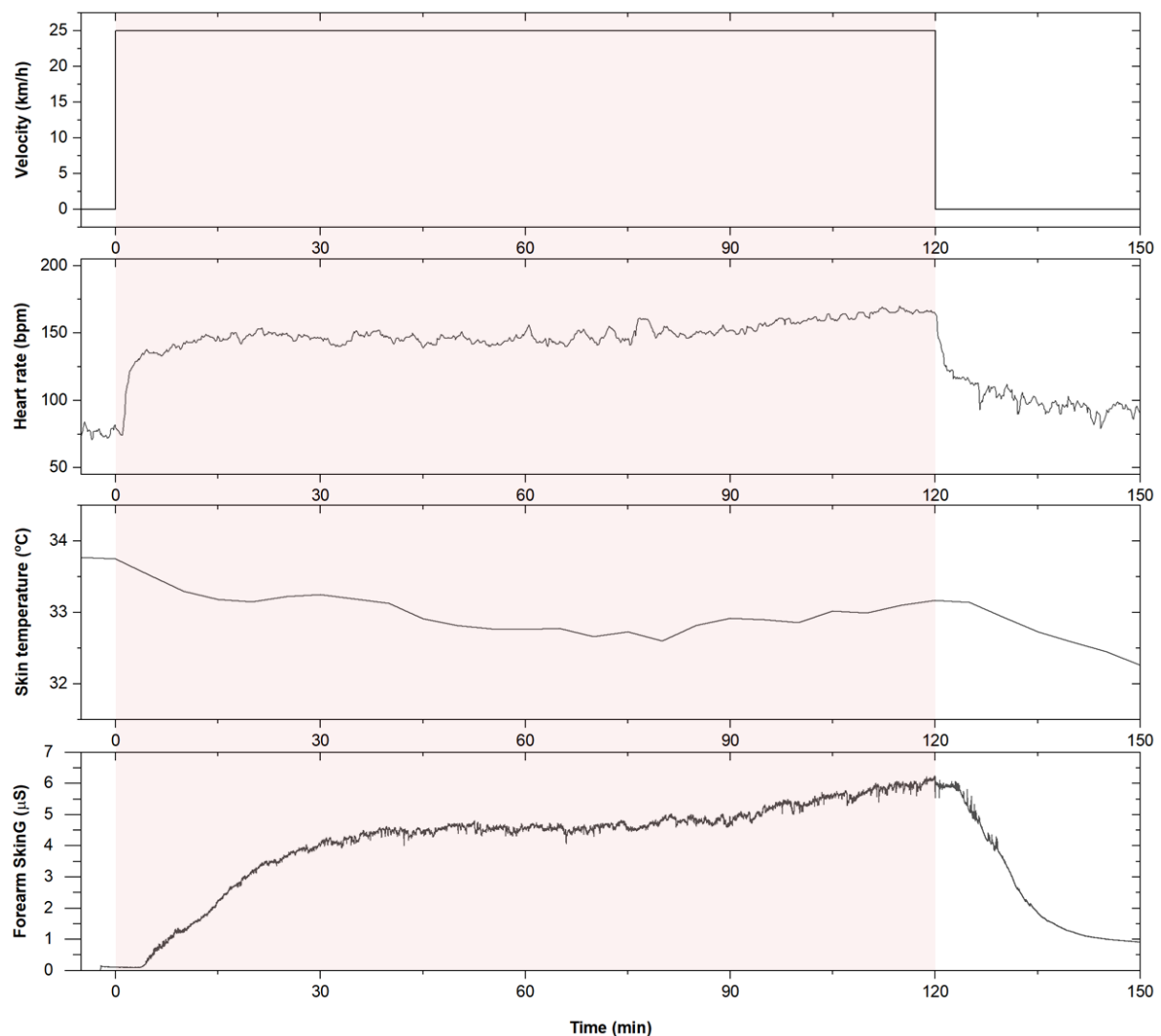
**Supplementary Figure 9 | Heart rate, skin temperature, SkinG changes during running on the treadmill.**



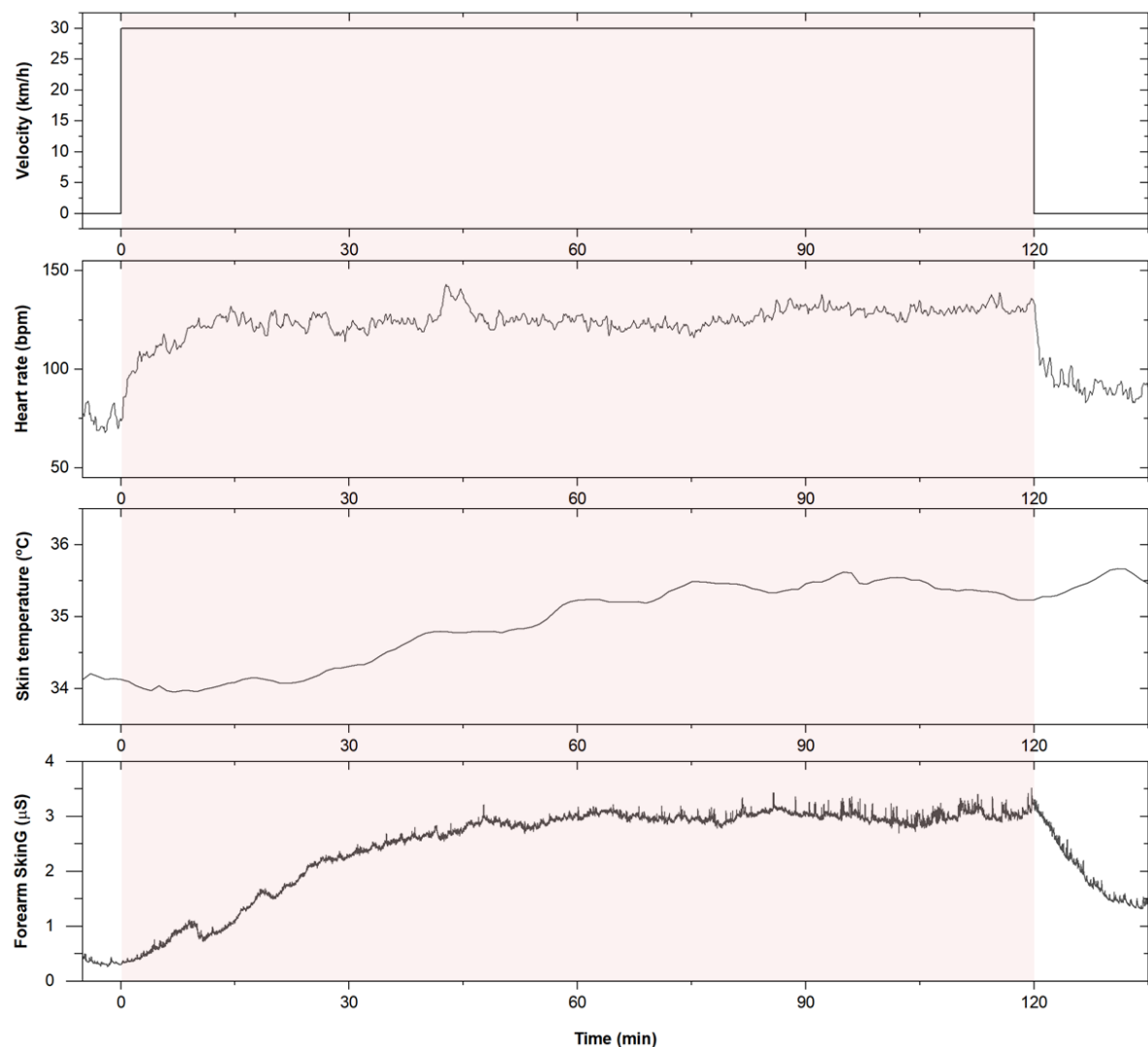
**Supplementary Figure 10 | SkinG variations using standard commercial Ag/AgCl electrodes.** Using standard commercial Ag/AgCl electrode (a, Scale bar: 5 mm), (b) SkinG variations on fingertip at rest and (c) SkinG recovery responses on the upper arm after 15 minutes of riding a stationary bike were measured.



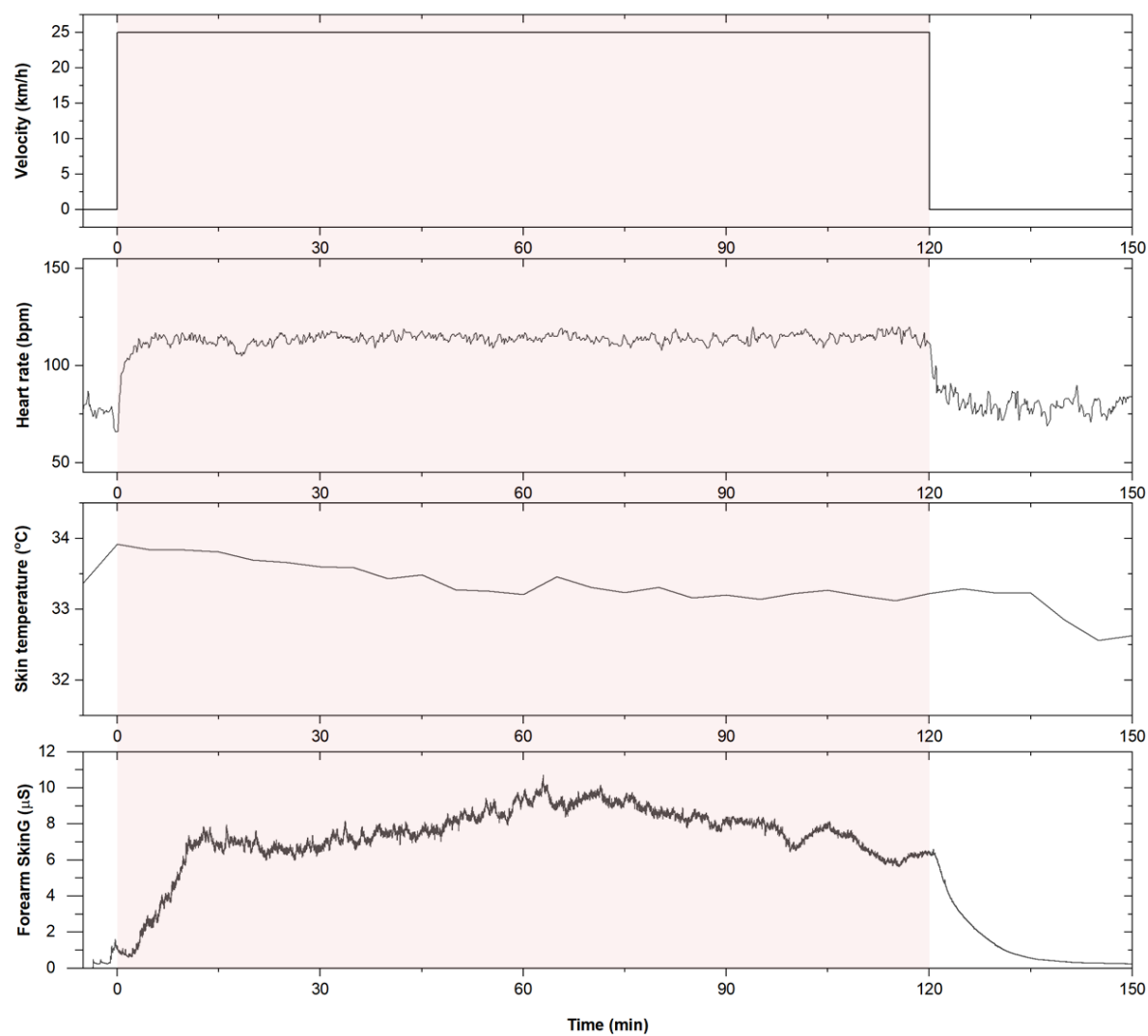
**Supplementary Figure 11 | SkinG changes of the same subject with increasing bike speed.**



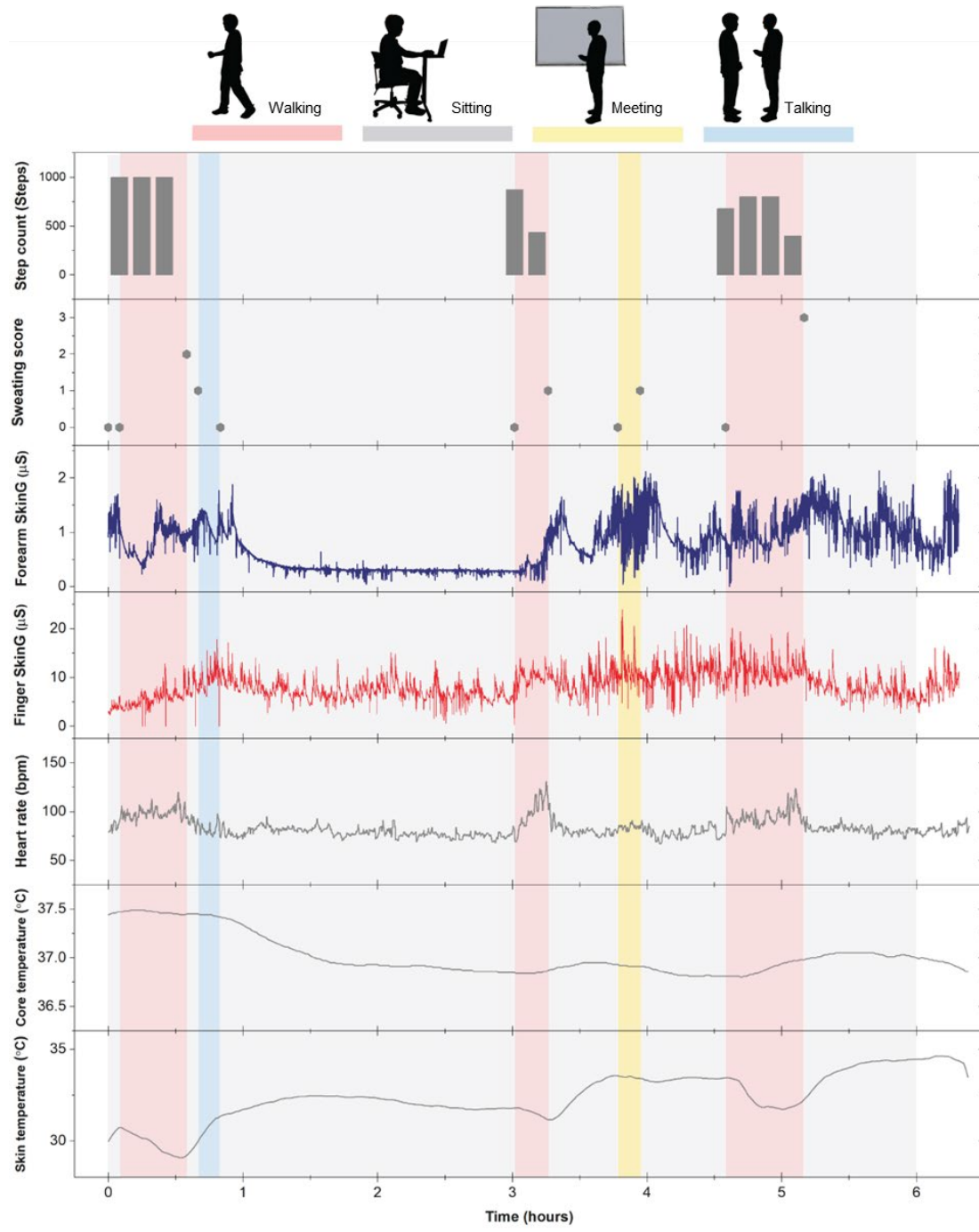
**Supplementary Figure 12 | Heart rate, skin temperature, and forearm SkinG profiles during 2 hours of stationary cycling: SkinG with increasing phase over time.**



**Supplementary Figure 13 | Heart rate, skin temperature, and forearm SkinG profiles during 2 hours of stationary cycling: SkinG with stable phase over time.**

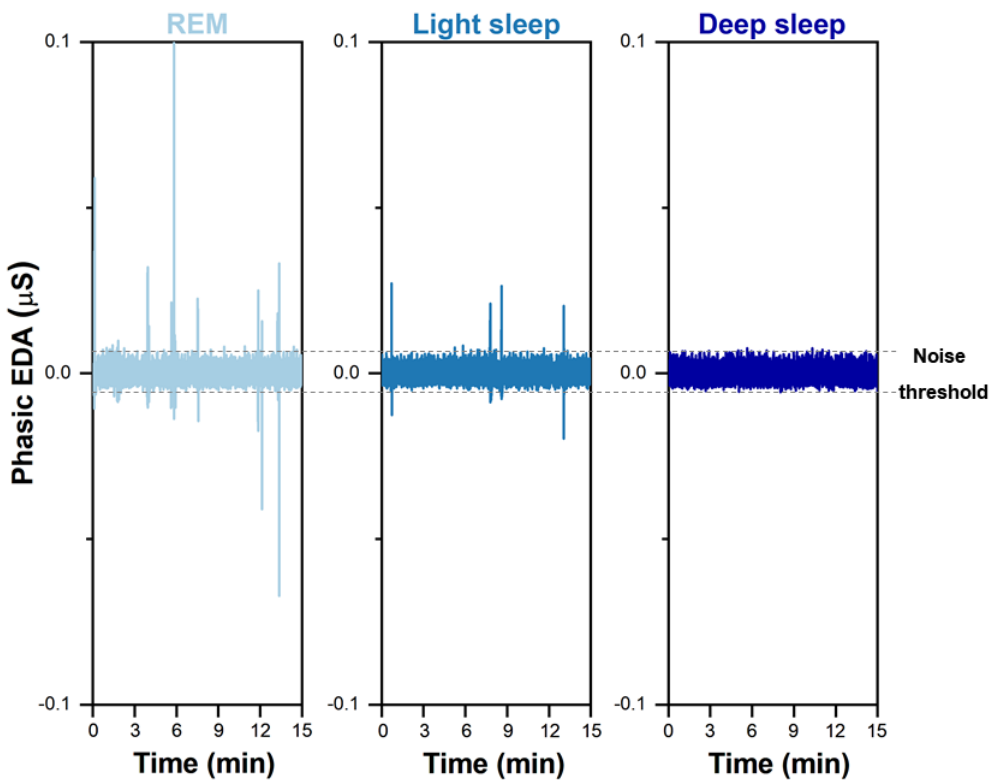


**Supplementary Figure 14 | Heart rate, skin temperature, and typical forearm SkinG profiles during 2 hours of stationary cycling: SkinG with decreasing phase over time.**

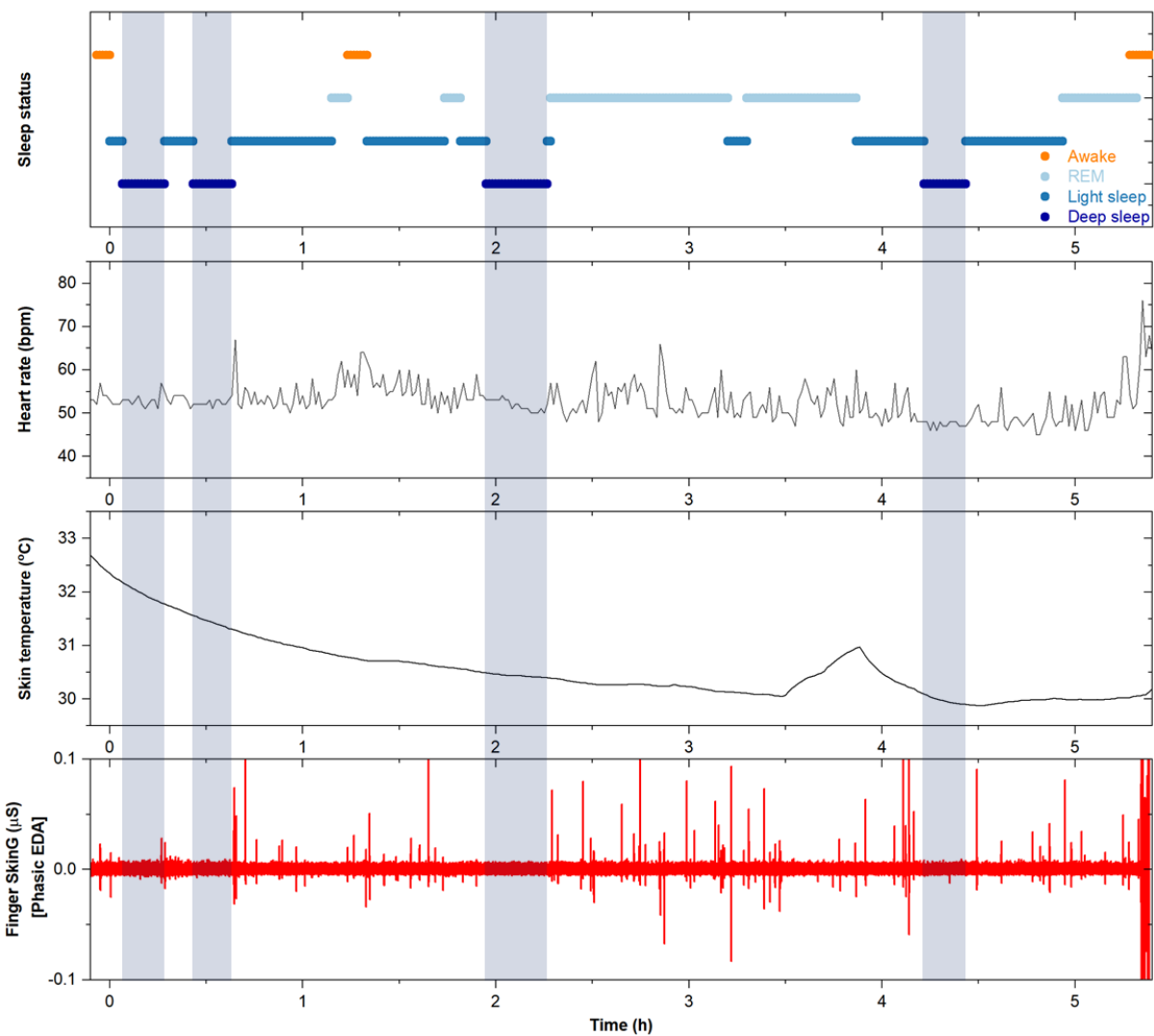


**Supplementary Figure 15 | Long time monitoring of SkinG using standard commercial**

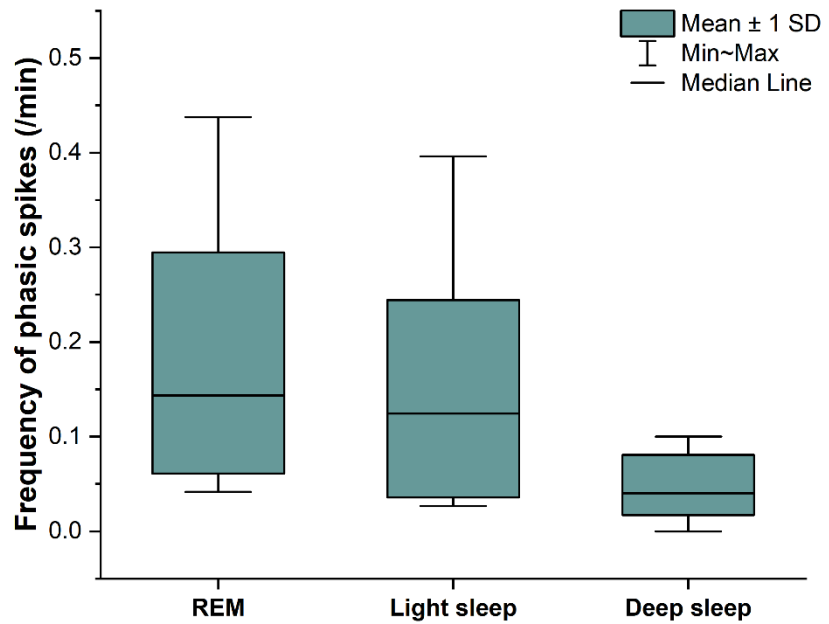
**Ag/AgCl electrodes.** A subject wore two SkinG sensors of non-permeable Ag/AgCl electrodes on the forearm and fingers, an activity tracker on the wrist, and a temperature sensor on the wrist during 6 hours of daily activities (walking, sitting, meeting, and talking). Also, the subject qualitatively scored their sweat rate on a scale from 0 to 3.



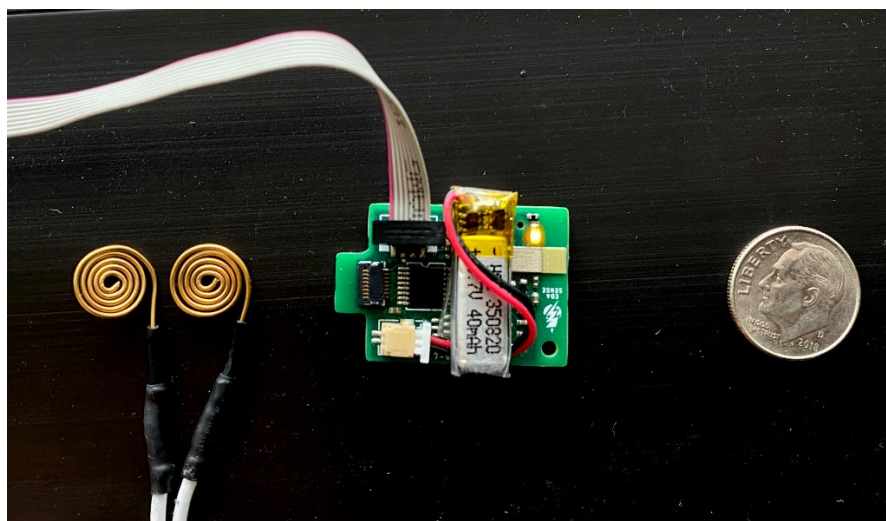
**Supplementary Figure 16 | Representative phasic EDA waveform from the finger during sleeping.** The number of phasic spikes was calculated by setting a noise threshold.



**Supplementary Figure 17 | Sleep status, heart rate, skin temperature, and phasic EDA from finger SkinG data during sleeping.**

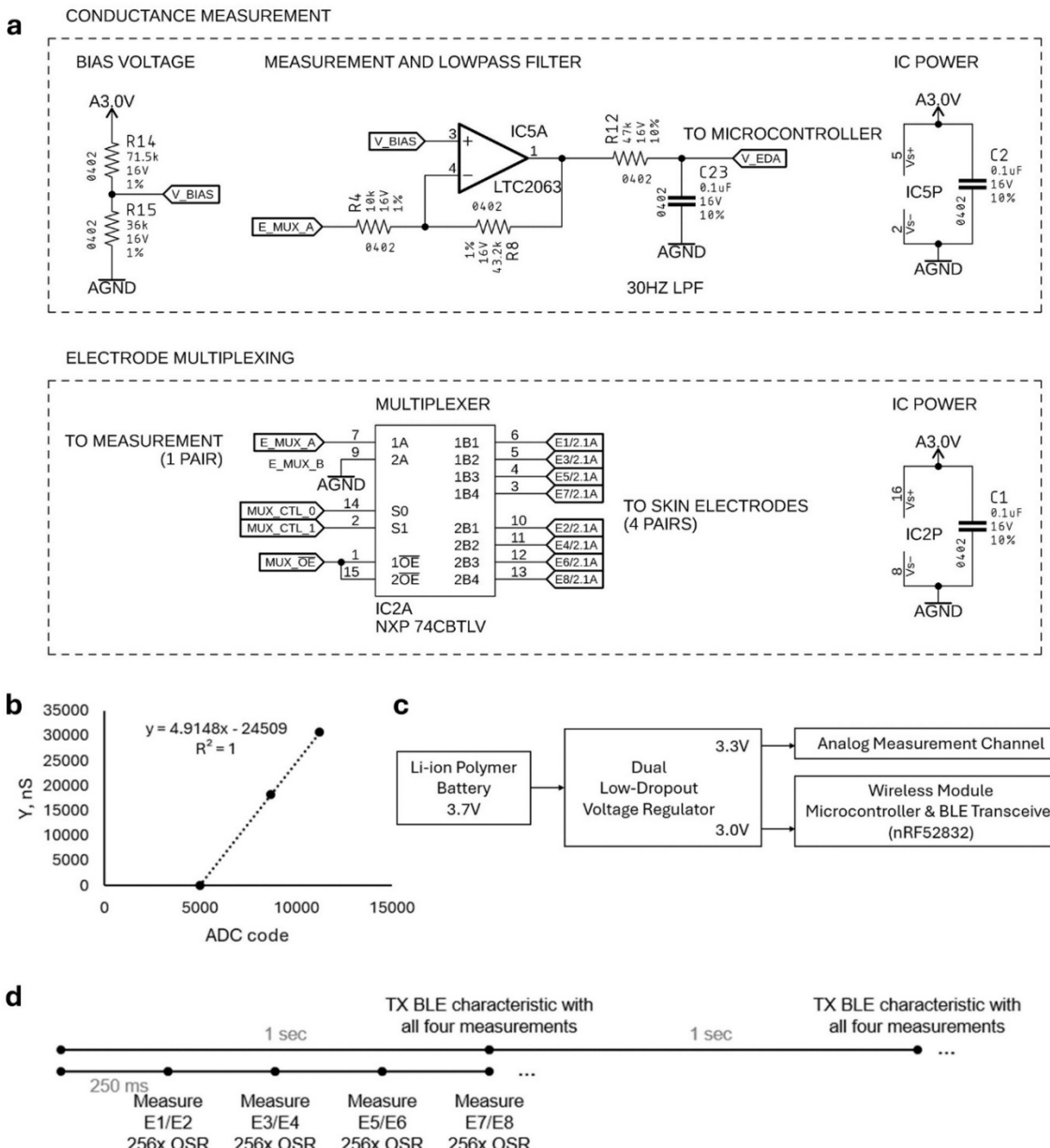


**Supplementary Figure 18 | Frequency of phasic spikes from finger SkinG recorded during 12 nights of sleep in one subject.**

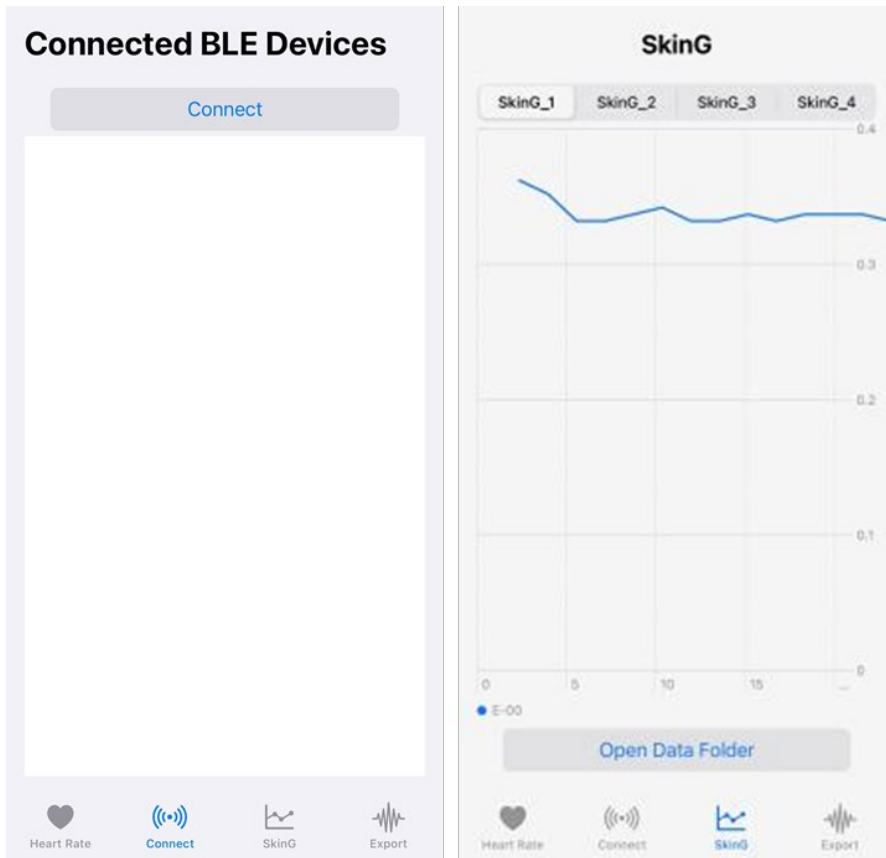


**Supplementary Figure 19 | Photograph of integrated SkinG multiplexed sensing system.**

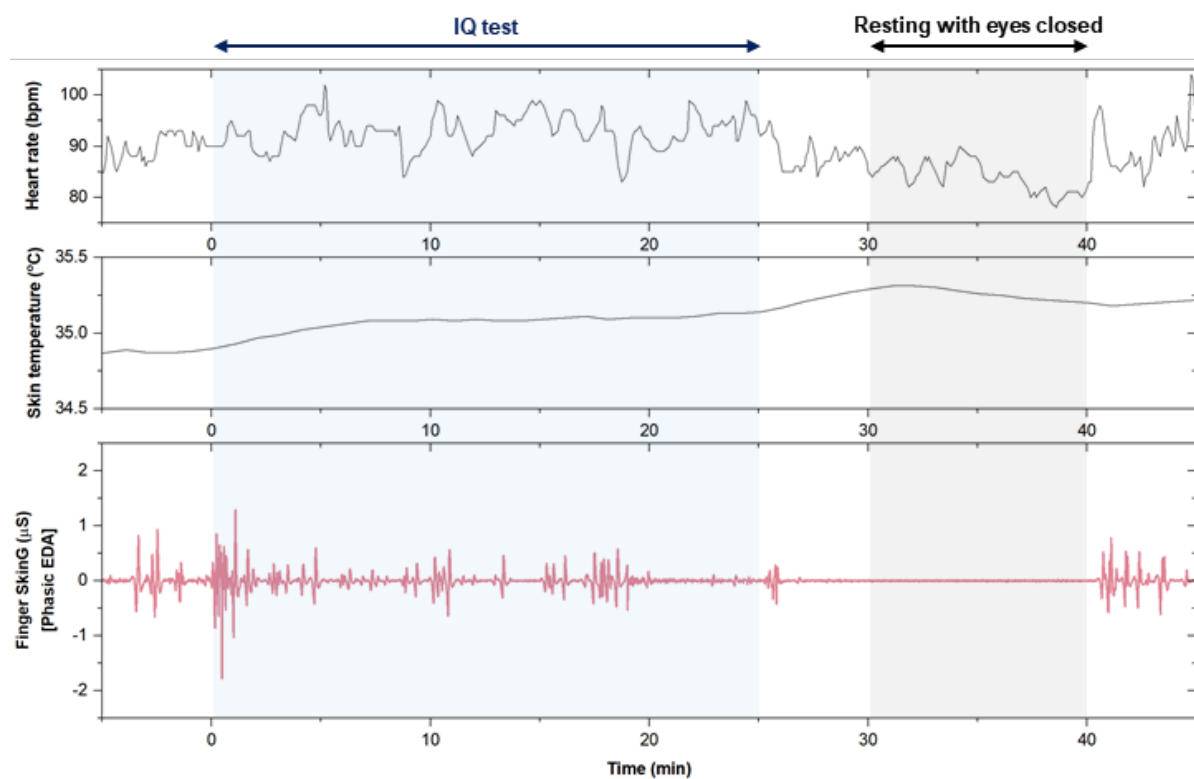
The printed circuit board is shown with an attached rechargeable battery module and 8-conductor connecting cable for up to four pairs of sensing electrodes, one pair of which is shown in the image.



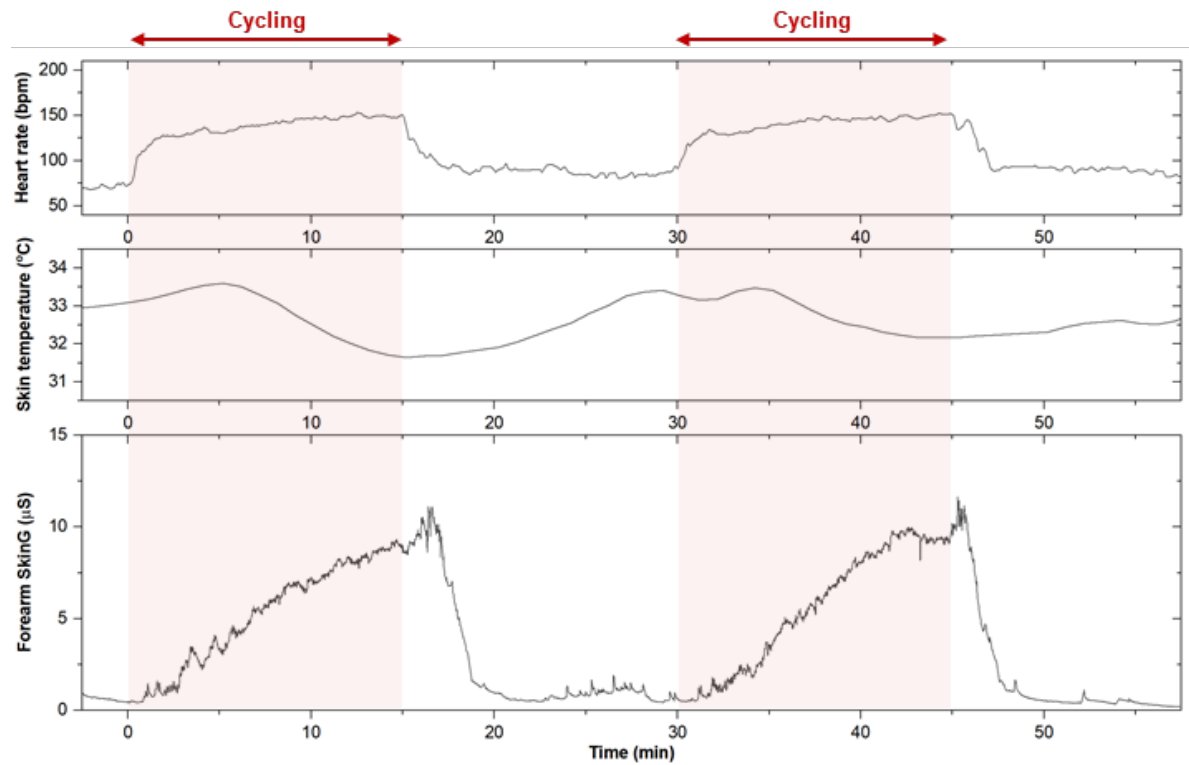
**Supplementary Figure 20 | Design of SkinG printed circuit board for multiplexed wireless sensing.** **a**, Circuit schematic of conductance measurement channel. **b**, Calibration of conductance measurement from microcontroller ADC code readout. **c**, Power delivery to analog and digital circuitry. **d**, Diagram of timing for measurement multiplexing, oversampling, and wireless data transmission.



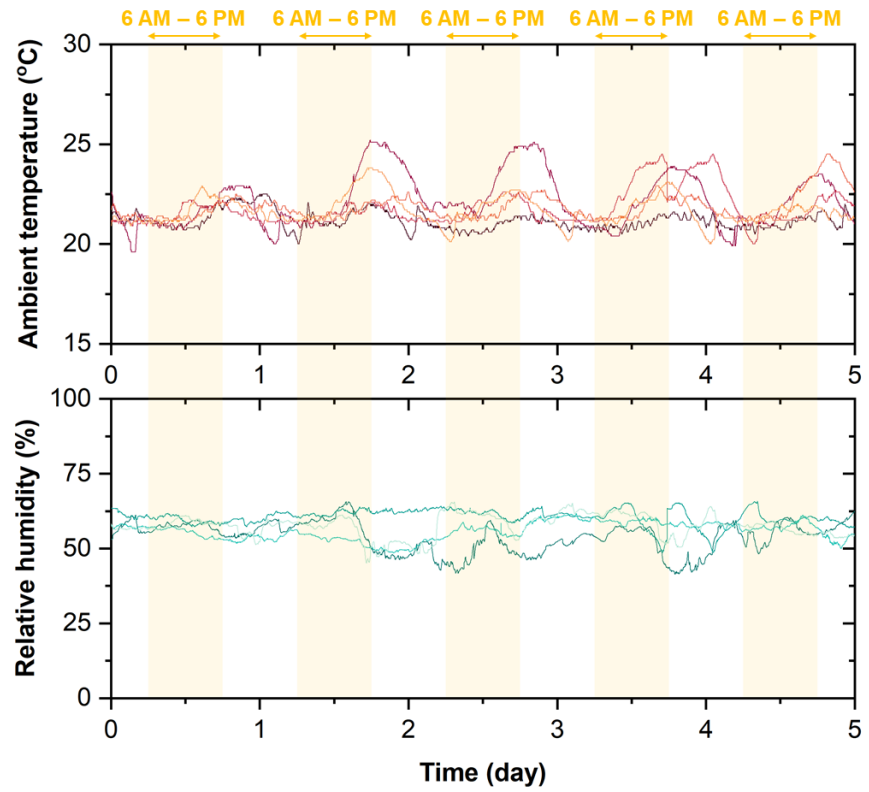
**Supplementary Figure 21 | The custom iOS mobile application for data display and export.**



**Supplementary Figure 22 | Heart rate and skin temperature changes during mental activities compared with phasic EDA from the finger SkinG.**



**Supplementary Figure 23 | Heart rate and skin temperature changes during physical activities compared with the forearm SkinG.**



**Supplementary Figure 24 | Ambient temperature and relative humidity on weekdays for 5 weeks in controlled laboratory with ventilation.**

**Supplementary Table 1 | Comparison of studies measuring physical activity using Sk inG.**

References	Electrodes	Permeability	Body locations	Physical activities	Responses	Baseline recovery
16	Hydrogel + Silver/silver chloride sheet	X	Finger	Walking, Running	Tonic, Phasic	-
17	Silver/silver chloride point probe	Intermittent measurement	Finger	Cycling	Average	Y
18	Stainless steel sheet	X	Finger	Cycling	Average	N
15	Electrolyte gel + Silver thin-film	X	Wrist	Walking, Cycling	Phasic	N
19	Gold thin-film	X	Wrist, Shoulder	Walking	Phasic	N
12	Graphene	O	Palm	Walking, Running	Phasic	Y
<b>This work</b>	$\mu$ -lace gold thin-film, Spiral stainless steel (or gold) wire	O	Wrist, Forearm, Upper arm	Walking, Cycling, Running	Tonic	Y

**Supplementary Table 2 | 43 data points in Figure 4b for calculating confidence interval**

(i: index, x: local sweat amount, y:  $\Delta\text{SkinG} / \text{SkinG}_o$ ,  $\bar{x}$ : average of x).

$5.92 \leq m \leq 9.52$  (with 95% confidence interval)

$$[m_1 \pm t_{\alpha/2, n-2} \cdot \{\sum(y_i - \hat{y}_i)^2 / (n - 2)\}^{1/2} / \{\sum(x_i - \bar{x})^2\}^{1/2} = m_1 \pm t_{0.05/2, 43-2} \cdot \{\sum(y_i - \hat{y}_i)^2\}^{1/2} / (43 - 2)]^{1/2} / \{\sum(x_i - \bar{x})^2\}^{1/2} = 7.72 \pm 2.019 \cdot (22999.70087 / 41)^{1/2} / (702.51817)^{1/2} = 7.72 \pm 1.80]$$

i	x	$x_i - \bar{x}$	$(x_i - \bar{x})^2$	y	$\hat{y} = 7.72x$	$y_i - \hat{y}_i$	$(y_i - \hat{y}_i)^2$
1	3.86667	-0.3079	0.0948	20.05263	29.85067	-9.79804	96.00149
2	0.33086	-3.8437	14.77406	14.85714	2.55427	12.30287	151.36064
3	4.5284	0.35383	0.12519	54.37313	34.95921	19.41392	376.90046
4	7.99506	3.82049	14.59617	127.68421	61.72188	65.96233	4351.0295
5	19.99012	15.81556	250.13179	160.42857	154.32375	6.10482	37.26881
6	5.99506	1.82049	3.3142	87.65979	46.28188	41.37792	1712.13204
7	11.3284	7.15383	51.17724	121.08955	87.45521	33.63434	1131.26899
8	5.41728	1.24272	1.54434	29.83333	41.82143	-11.9881	143.71451
9	6.26298	2.08841	4.36147	78.78639	48.35023	30.43616	926.35983
10	0.66173	-3.51284	12.34004	6.44681	5.10854	1.33827	1.79095
11	3.73333	-0.44123	0.19469	7.11388	28.82133	-21.70745	471.21357
12	0.8	-3.37457	11.38771	8.25234	6.176	2.07634	4.31117
13	1.06667	-3.1079	9.65905	20.40351	8.23467	12.16884	148.08072
14	0.4642	-3.71037	13.76685	6.3224	3.5836	2.7388	7.50102
15	4.73086	0.5563	0.30947	19.73394	36.52227	-16.78833	281.84791
16	3.73333	-0.44123	0.19469	10.8125	28.82133	-18.00883	324.31808
17	0.8	-3.37457	11.38771	3.80488	6.176	-2.37112	5.62222
18	2.33086	-1.8437	3.39924	11.14765	17.99427	-6.84662	46.87621
19	0.8642	-3.31037	10.95855	3.59259	6.6716	-3.07901	9.48032
20	0.26667	-3.9079	15.27169	5.83333	2.05867	3.77467	14.24811
21	1.46667	-2.7079	7.33273	8.74026	11.32267	-2.58241	6.66883
22	0.33314	-3.84143	14.75659	3.57143	2.57182	0.99961	0.99922
23	2.19871	-1.97586	3.90403	12.32322	16.97401	-4.65079	21.62989
24	0.8	-3.37457	11.38771	9.78947	6.176	3.61347	13.05719
25	2.93333	-1.24123	1.54066	21.77778	22.64533	-0.86756	0.75265
26	4.5284	0.35383	0.12519	65.88525	34.95921	30.92604	956.4197
27	7.99506	3.82049	14.59617	24.33333	61.72188	-37.38854	1397.90316

28	7.7284	3.55383	12.62969	33.89362	59.66321	-25.76959	664.07192
29	7.86173	3.68716	13.59515	54.71429	60.69254	-5.97826	35.73956
30	3.99506	-0.17951	0.03222	22.26667	30.84188	-8.57521	73.53422
31	2.26667	-1.9079	3.64009	16.95	17.49867	-0.54867	0.30104
32	7.06173	2.88716	8.33569	20.06509	54.51654	-34.45145	1186.90271
33	0.26651	-3.90806	15.27292	31.34313	2.05746	29.28568	857.65079
34	5.06173	0.88716	0.78705	46.8022	39.07654	7.72565	59.68574
35	2.66667	-1.5079	2.27377	26.39583	20.58667	5.80917	33.74642
36	0.33086	-3.8437	14.77406	29.25641	2.55427	26.70214	713.00421
37	1.46667	-2.7079	7.33273	66.7907	11.32267	55.46803	3076.70246
38	13.85679	9.68222	93.74542	94.07042	106.97442	-12.904	166.51314
39	0.53333	-3.64123	13.25859	19.23077	4.11733	15.11344	228.41594
40	1.06667	-3.1079	9.65905	10.37093	8.23467	2.13626	4.56362
41	8.66157	4.487	20.1332	20.06216	66.86733	-46.80517	2190.72432
42	5.92985	1.75528	3.081	55.00558	45.7784	9.22718	85.14083
43	5.3302	1.15563	1.33548	9.50991	41.14913	-31.63922	1001.04003

**Supplementary Table 3 | SkinG board measurement characteristics.**

EDA measurement type <i>(endosomatic, exosomatic; applied V, applied I; DC, AC)</i>	Exosomatic with applied DC voltage
Applied voltage between electrodes	approximately 1 V $1V \times R_{skin}/(R_{skin}+10k \Omega)$
Measurement multiplexing	4 pairs of electrodes
Measurement output rate	1 Hz
Oversampling ratio	256x

**Supplementary Table 4 | SkinG board safety.**

Applied voltage	< 1 V
Applied current  Maximum of 1 V through minimum of 10k $\Omega$ (current-limiting resistor)  <i>Human perception threshold is 1 mA</i>	< 100 $\mu$ A

**Supplementary Table 5 | SkinG board measurement range.**

	Min	Max
Absolute range of wireless PCB	0 $\mu$ S  Applied voltage: 1V	32.7 $\mu$ S  Applied voltage: 0.75V
Typical human skin conductance	1 $\mu$ S  Applied voltage: 0.99V	20 $\mu$ S  Applied voltage: 0.83V